ASTRONOMY & ASTROPHYSICS
SUPPLEMENT SERIES

JULY 1989, PAGE 79

Astron. Astrophys. Suppl. Ser. **79**, 79-103 (1989)

Infrared observations of the Magellanic Clouds. I. The Small Magellanic Cloud

P. B. W. Schwering(*) and F. P. Israel

Sterrewacht Leiden, Huygens Laboratorium, Niels Bohrweg 2, Postbus 9513, NL-2300 RA Leiden, The Netherlands

Received May 4, 1987; accepted February 28, 1989

Summary. — Results of IRAS pointed observations in four infrared wavelength bands (12, 25, 60 and 100 μm) on the Small Magellanic Cloud are presented. Maps with orthogonal scan directions are shown and a source list containing 219 infrared sources is extracted from the data. Comparison with the IRAS Point Source Catalog (PSC) shows that only three entries in this catalogue are spurious. Thirty-three of the sources found (and listed in the PSC) are extended. We confirm all 13 entries in the IRAS Small Scale Structure Catalog (SSS) in the SMC. We found 72 new infrared sources, not included in either the PSC or in the SSS. Our SMC infrared source list is compared to other object lists. We identified 28 SAO stars, two blue globular clusters and seven planetary nebulae. We did not find any SMC-stars nor did we find a clear correlation with supernova remnants. In general there is a good correlation of infrared emission with the distribution of HII regions and dark clouds. Results of infrared maps of two additional fields at the SE and SW corners of the SMC are presented in an Appendix, together with a list of sources that were extracted from these maps.

Key words: infrared radiation — stars: formation of — HII-regions — Galaxies: Magellanic clouds.

1. Introduction.

The Magellanic clouds are the closest galaxies in the Local Group. In fact, with distances D= 53 kpc (LMC) and D = 63 kpc (SMC ; Humphreys, 1984) they are the nearest (dwarf) irregular galaxies. As a result, with the same instrument linear resolutions on the Magellanic Clouds are of order 50 times better than those on comparable other blue dwarf irregulars, thus enabling terrestrial observers to conduct extensive studies on their detailed structure. Compared to the Solar Neighbourhood, both Magellanic Clouds are characterized by low dust and low heavy-element abundances (see e.g. the review by Israel, 1984). Relatively high present-day star formation rates, hence the presence of large number of luminous hot stars, nevertheless lead to significant infrared emission from warm dust. Only limited infrared information on the Clouds is available from ground based and airborne observations (see Tab. I). All these observations were limited to the brightest *a priori* known objects and covered negligible fractions of the Cloud surfaces. A complete infrared survey of the Magellanic Clouds was first obtained by the Infrared Astronomical Satellite (IRAS). The IRAS mission (IRAS, 1985a) produced a list of point sources over the whole sky, including the clouds, as well as a series of maps, both in the Survey mode and in pointing modes, and a catalogue of Small Scale Structure (SSS). However, the IRAS Point Source Catalog (PSC) entries for the Clouds in principle suffer from confusion. Potential effects of this on the PSC are artificial detections and missed real sources. Maps of the sky brightness as observed by IRAS in the 16?5 extended emission images (Skyflux) and the Additional Observations (AO) program, give better information about (point and extended) sources in the Magellanic Clouds, because they represent two-dimensional images, while the PSC was obtained from one-dimensional detector datastreams. The advantage of the AOs over the 16?5 skyflux images is the higher resolution, better sampling, better pointing, higher sensitivity and less striping. Because of the position of the Clouds near the Ecliptic Pole many different scan angles occur which fill the present Skyflux maps with radial striping. Due to this striping and other background variations determination of good fluxes for both Magellanic Clouds from the Skyflux

(*) *Present address:* Infrared Group, Physics and Acoustics Division, TNO Physics and Electronics Laboratory, P.O. Box 96864, 2509 JG Den Haag, The Netherlands.

Send offprint requests to: P. B. W. Schwering.

maps is very difficult, especially at 12 μm. Here we present full-resolution AO maps of the SMC and information on discrete sources extracted from these maps.

2. Observations and data reduction.

The observations presented in this paper were obtained with the IRAS satellite as part of the AO program carried out with the IRAS survey array. A full description of the instrument array, the survey and data processing can be found in the IRAS Explanatory Supplement (IRAS, 1985a). A description of the AO program and a list of all rasterscan AOs observed by the IRAS satellite of many different objects are given in "*A User's Guide to IRAS Pointed Observation Products*" (IRAS, 1986).

There is a variety of pointed observations on the SMC (see Israel and Schwering, 1986). Most of them (IRAS AO observation technique DPS) cover an area of $1\overset{\circ}{.}5 \times 0\overset{\circ}{.}5$, others (DSD) are useful only for small fields on selected objects. Deep Sky Mapping (DPM) observations are the only ones covering the entire SMC in a regular manner. Because these DPM observations are not limited by noise and the resolution cannot be improved by adding the other AO observations, it was decided not to combine observations obtained with different observing techniques. This also avoided possible problems in combining these different AOs, and in having inhomogeneous coverage of the SMC. The maps presented here are thus based on the DPM observations alone. The observations were made in the months of June, July and September 1983, and are summarized in table II.

In the DPM mode, a rasterscan of 6 or 7 legs of $166'$ length was made with a cross-scan step of $20'$, while scanning took place in the normal survey direction. Scanning each leg took about 43 seconds with a turnaround time of about 17 seconds, so that observing a single DPM field took about 8 minutes. The scan speed was $3\overset{'}{.}85$/sec, as for the survey. Compared to the survey the signal-to-noise ratio increased by a factor of about 1.4.

Deliberately two separate sets of DPM observations were made with almost orthogonal scanning directions : approximately EW and NS. This was possible because the SMC is close to the South Ecliptic Pole ($\beta_{SMC} = -65°$), so that observations obtained three months apart yielded the required orthogonal scanning directions. Due to the rectangular form of the IRAS survey detectors (largest size in the cross-scan direction) the resolution is highest in the scan direction (timeresolution), so that these two sets of data supply us with maximum resolution in both directions. In June the SMC was scanned NS (average position angle of the scan direction 159° ; observations set 1 NS in Tab. II) in a double coverage, in July also NS (173° , set 2 NS) with a coverage of four. In September (three months later) the SMC was scanned EW (253° ; set 3 EW) with double coverage. Because of the large size of the SMC compared to the area covered by a single DPM observation every coverage consists of four differently pointed observations. Another nine observations were made (two in June and seven in July) , which were processed and later deleted for various reasons (see below).

The reduction was done in two stages. The first stage of data reduction took place at the IRAS Science Data Analysis System (SDAS). It contained the stim-flash calibration of the detector datastreams (see IRAS, 1985a) to the IRAS May 1984 standard. Dead detectors and the smaller edge-detectors were left out to obtain a consistent sampling for small sources. Detector offsets were eliminated to avoid detector striping in the maps (Kopan, 1984). Because each individual detector had its own gain characteristics and inconsistencies between different detectors in a single band remained, an unacceptably high striping level may result unless special care is taken. The method used reduced the stripes very effectively to a reasonably low level (but non-zero) by positionally aligning detector datastreams in-scan, histogramming the difference between each pair of adjacent detectors, identifying the mode of the histogram and subtracting the integrated mode for each detector datastream, while demanding the average subtraction over the whole DPM field to be zero. These datastreams were then combined with the pointing information and subsequently gridded to a spatial matrix of 3° (in-scan) × 2° (cross-scan) with pixels of $2\overset{'}{.}0$ in the cross-scan direction and respectively $0\overset{'}{.}25$, $0\overset{'}{.}25$, $0\overset{'}{.}50$ and $1\overset{'}{.}0$ in the scan direction in the 12, 25, 60 and 100 μm bands by using standard software (Deep Sky Co-add Observation Processor DSCO ; Kopan, 1982). Detector data were co-added to each grid cell whose centre falls within the detector size. This grid matrix represents the infrared surface brightness in the four IRAS wavelength bands. Only non-filtered intensity grids were produced so that flux information is preserved. We obtained 41 individual DPM grids on the SMC in this way (see Tab. II).

The second stage of the processing, done at Leiden Observatory, consisted of combining individual DPM grids, and obtaining a qualitatively and quantitatively good final product. First, quality checks brought to light that one of the SMC DPM grids (number 5851 in Tab. II) has degraded pointing reconstruction. To get an equal coverage of each area of the SMC, eight other grids were left out. The remaining 32 grids then were used to obtain three combined map sets (in four wavelength bands) of the whole SMC (each map covers an area of $4\overset{\circ}{.}3 \times 4\overset{\circ}{.}3$ with a grid spacing of $0\overset{'}{.}25 \times 2\overset{'}{.}0$; the two map sets that have their scan direction in constant Right Ascension are denoted by NS and the map set with scan direction in constant Declination by EW ; table II also shows which grid numbers were combined into each map set). These combined maps were made using standard SDAS software (Deep Sky Grid Adding Processor DSGAD ; Kopan, 1982). This first converts all individual grids to the same reference map and then adds all grids together weighting global noise for minimum variance and matching overlapping areas of individual grids.

The SMC is positioned at high ecliptic latitude so that there is little variation in the Zodiacal light emission over the maps. Nevertheless, some Zodiacal emission is

still present and can be clearly seen on the IRAS 16°.5 Skyflux images : levels of about 13 and 28 MJy/sr at 12 and 25 μm, and much less at 60 and 100 μm (about 5 MJy/sr). The galactic latitude of the SMC is $-44°$ so that the Galactic foreground, is weak (8 MJy/sr at 100 μm, much less at other wavelengths). At the 60 and 100 μm wavelengths the Galactic foreground cirrus gives more severe problems than the Zodiacal foreground because the Galactic foreground dust is colder. These large scale, relatively smooth foregrounds were removed in a somewhat arbitrary fashion by fitting a plane to map areas considered to be free of SMC emission. Discrete non-SMC sources, such as foreground stars, were not removed from the maps. Our zero-level correction removes most of the foreground emission but assumes a planar foreground, which is only a first order approximation of the foreground. In section 3 we describe the uncertainties that are left in the map after the foreground removal.

To finally bring the IRAS AO (DPM) data to the current (IRAS November, 1984 standard) calibration – the same calibration as the released primary IRAS products – we produced pixel-by-pixel scatterdiagrams of the DPM maps versus the Skyflux HCON-1 maps (the only one available at that time) at a resolution of 9′. Because a pixel-to-pixel correlation was required here, the slope of the diagram yields the necessary correction factors to arrive at the November 1984 calibration; these factors have an estimated relative uncertainty of about 10 % and correspond well to those communicated to us by Kopan (priv. comm.) obtained in a different manner using many more AOs on NGC 6543 (IRAS Primary Photometric Reference, positioned near the North Ecliptic Pole). The error of 10 % gives a good estimate of the reliability of the IRAS data on any point in the map. The correction factors are in principle affected somewhat by positional and flux errors in both the Survey derived and AO DPM derived maps. We have empirically corrected for most of the positional errors by determining the (Skyflux HCON-1)/(DPM AO) intensity ratios with a beam large compared to position uncertainties and applying small shifts to minimize scatter in the pixel-to-pixel correlation. This method was very succesful on the LMC ; on the SMC severe striping in the Skyflux data made this method more difficult to use at 12 and 25 μm, but the factors that we found did not differ much from those of Kopan, and therefore we used his factors in those wavelength bands.

3. The maps of infrared radiation.

Figure 1 shows a 100 μm map of the SMC, the LMC and their surroundings, constructed from Spline-I maps (van Albada *et al.*, 1985) by Braun, Walker and Deul at Leiden Observatory (taken from their collection of sky maps, see also Burton *et al.*, 1986). At the top the southern part of the Milky Way is visible (dust clouds associated with the Carina Arm at the top right, with peak intensities around 5000 MJy/sr). The LMC is just below the centre (l = 280°, b = −33°). The SMC (l = 304°, b = −44°) is seen at the bottom left, with a peak in the SW-Bar of only 42 MJy/sr. The diffuse SMC emission is at a level of 11 and the Galactic foreground of 8 MJy/sr. From the figure, it is clear that the Galactic infrared foreground at the position of the SMC is not very complex and easy to remove.

Figures 2 and 3 show IRAS DPM-maps of the whole SMC field. In these figures we indicate the boundaries of the coverage of the IRAS DPM observations. The NS (set 2) and EW (set 3) scanned maps are shown because the resolution in the scan direction is higher than the cross-scan resolution ; thus, the two (NS and EW) sets are complementary in terms of resolution. Map set 1 is very similar to map 2. There is less diffuse emission present in the 12 and 25 μm maps than in the other wavelength bands. In these maps the contrast between small, discrete sources and the diffuse more extended emission is much higher ($\sim$ 40) than at 60 or 100 μm ($\sim$ 10). The coverage of the SMC is not complete in the SE, where the HII-region N 90 is just outside of the map. Because HII region N 3 is just at the edge at the SW, good fluxes cannot be obtained for this source. Special Co-adds of IRAS Survey data have been done centered on these two objects and are presented in Appendix A.

Detailed maps in four fields on the SMC are presented in Schwering and Israel (1989) and are available in digital form at the Centre de Données Stellaires (Astronomical Data Centre CDS) in Strasbourg, France.

All maps shown in this paper are given in in-band intensities $\int d\nu\, R_\nu I_\nu$ (Watt m^{-2} sr^{-1}), with R_ν the relative system response (see IRAS, 1985a ; Tab. II.C.5 therein). To convert these values to specific intensities I_ν (Watt m^{-2} sr^{-1} Hz^{-1}) correction factors should be applied depending on the bandwidth (these factors are given in table III, assuming an intrinsic source spectrum $f_\nu \propto \nu^{-1}$, which is roughly correct for most dust clouds associated with HII regions : $T_d \approx 40$ K). For individual sources or positions, more accurate flux densities can be obtained by first determining the actual spectrum and then applying the relevant colour dependent correction (see IRAS 1985a and IRAS 1985b, Tab. VI.C.6 therein).

The estimated uncertainties in the DPM maps are given in table III. There are only minor differences in quality of the three different sets of maps. The noise (in MJy/sr) in the maps increases in the higher wavelength bands. Because the noise is based on map statistics, this is due to the increased extended emission of the SMC itself. The zero-level is also less well defined in those bands due to the extended emission. The sensitivity is based on reliable point sources that could be extracted from the maps. Just North of the SMC-Bar in map set 1, a bad detector scan makes that part of the map unusable, but as it falls completely outside the SMC it does not hamper the interpretation of the data.

4. The Infrared Source List in the SMC.

4.1 The Source List. — We searched the three sets of maps for both resolved and unresolved discrete sources (Tab. IV) down to intensity levels of 5, 2, 1 and 0.5×10^{-8} Watt

m^{-2} sr^{-1} at 12, 25, 60 and 100 μm (four times the median noise level). Intensity peaks, backgrounds and source sizes were estimated and used to obtain flux densities. The extended diffuse SMC infrared emission is also interpreted as background, whenever it was close to the source. A size estimate was obtained using the nominal Gaussian resolutions in the different bands. All wavelength bands and all three different map sets were searched separately. In a single wavelength band flux densities are about equal in the three maps, especially in unconfused regions (deviation of about 15 %). The data were then merged. The IRAS PSC positions are quoted in table IV whenever an unambiguous identification was made.

Table IV contains the following information :

column 1 : sequential number. We recommend the name LI-SMC for these sources (Leiden IRAS-SMC).

column 2 : the position of the source (1950). The Right Ascension is given in hours, minutes and seconds. If given in 0.1^s the position and error are that of the IRAS PSC entry given in column 12, otherwise they are taken from the maps with an error of 12^s. The declination is given in degrees, arc-minutes and arc-seconds. If given in $1''$ the position and error are that of the IRAS PSC entry given in column 12, otherwise they are taken from our maps and have an error of $1'$.

column 3 : 12 μm intensity peak and background level (in 10^{-8} Watt m^{-2} sr^{-1}). A dash indicates that the source is below the intensity level given in the text.

column 4 : the same as column 3 for the 25 μm band.

column 5 : the same as column 3 for the 60 μm band.

column 6 : the same as column 3 for the 100 μm band.

column 7 : the size of the source in $\alpha(') \times \delta(')$. p denotes a source that cannot be discerned from a point source response. A semi-colon denotes an uncertain size. A dash indicates that no reliable size could be estimated because no FWHM could be determined.

column 8 : flux density of the source at 12 μm in Jy, assuming an intrinsic source spectrum $f_\nu \alpha \nu^{-1}$ (the same as for the released IRAS products ; IRAS, 1985a). C denotes confusion with either background or other discrete sources and a semi-colon indicates an uncertain flux density. Flux densities are calculated using the size of column 7. When the size could not be measured the point source response was assumed. Table III gives Point Source Conversion Factors to convert (Peak-Background) Watt m^{-2} sr^{-1} to Jy. The error in flux densities is assumed to be about 10 % , but somewhat higher at the lower intensity levels.

column 9 : the same as column 8 for the 25 μm band.

column 10 : the same as column 8 for the 60 μm band.

column 11 : the same as column 8 for the 100 μm band.

column 12 : if the source is present in the IRAS PSC (IRAS, 1985a) and/or in the IRAS SSS (IRAS, 1985b) the name in that catalogue is given. A semi-colon indicates that the associated PSC or SSS entry is at a large distance from the source. An asterisk indicates that the association has been made for more than one source in the list.

column 13 : the spectral type of the source. Spectrum type C is a typical cool dust spectrum (typical $T_d \approx 30$ K), peaking beyond 100 μm ; colour correction factors are of order 1.00, 0.95, 0.99, 1.00. Type W is a warm dust spectrum (typical $T_d \approx 70$ K), peaking between 12 and 100 μm ; colour correction factors are of order 1.03, 1.00, 1.00, 1.04. Type S is a stellar spectrum (typical blackbody of about 5000 K) ; colour correction factors are of order 1.43, 1.40, 1.32, 1.09. A semi-colon indicates that the infrared spectrum is uncertain. Actual flux densities can be calculated from the quoted ones by *dividing* the latter by these colour correction factors (see IRAS, 1985a).

column 14 : comments information on identification in other catalogues.

Our source list contains 219 entries. In the area covered by the DPM fields 146 entries were found in the IRAS PSC, of which 138 could be identified unambiguously. Five PSC sources can be identified, but show some positional difference (about $1'.4$). The remaining three PSC sources could not be identified on the DPM maps : IRAS 00515-7227, 01062-7210, 01098-7225, almost certainly because of confusion problems. The last (100 and 60 μm) source has a (second and correct, 25 μm) IRAS PSC entry at $1'.5$ distance (01095-7225). We believe that these two PSC entries are in fact the same source. The other two sources have reliable PSC flux densities at 60 μm only. They are probably the result of confusion in the SMC Bar (see below). IRAS 00296-7404 (HII region N 3) peaks just inside one DPM map and is detected at 60 and 100 μm. We left it out of the source list, because the coverage of the source is not very good. In total 33 PSC sources are clearly extended, and 60 are confirmed to be a point source. The source types in our list and in the PSC agree very well. Frequently, our procedure yields flux determinations where the PSC only gives upper limits.

All 13 entries in the IRAS SSS and inside the DPM fields were detected. Two of them (IRAS X0110-724 and X0112-735) are associated with more than one of our sources. The associations for IRAS X0110-724, X0115-737 and for X0123-736 are farther than $3'$ away. Nine SSS sources have an association with an entry from the PSC ; these must be sources with unresolved and extended components. The extended structure of the SMC at 60 and 100 μm is complicated, and therefore sometimes does the SSS entry merely represent just one part of it. There are 72 new infrared sources in this source list, not included in the PSC nor in the SSS. The IRAS High Source Density Bin data (IRAS 1985a) show that the condition of high source density exists at 100 μm over the whole SMC and at 60 μm in the SMC Bar. In these confused and high source density regions in the sky the IRAS PSC is constructed with the primary aim to be reliable, even when it means less complete. The majority of these new sources are point sources, and clearly

show the incompleteness of the IRAS PSC in confused areas.

4.2 POSITIONS. — The positions of the sources in the maps were compared with sources in the IRAS PSC. There was a good correspondence, that allowed us to use PSC coordinates for an unambiguous association. In the 12 μm map the correspondence with the known SAO star positions is very good (average deviation of 15″). We also compared the positions at a resolution of 9′ against the Skyflux HCON-1 maps. Compared to the Skyflux data there are small systematic position shifts of order of 1′ ($\frac{1}{2}$ Skyflux-pixel size), but because those shifts are not present when we compare the DPM maps with the PSC, this indicates that the positional accuracy in the DPM maps presented here is significantly better than that in the skyflux maps. Ground based near-infrared observations at La Silla (Israel *et al.*, 1988) indicate an overall mean accuracy of 10″ for IRAS point sources (PSC) in the Magellanic Clouds.

4.3 FLUX DENSITIES. — We compared the flux densities from the DPM maps with those from the PSC (version 1.0, November 1984). This is a comparison of independent data obtained with the same instrument, but reduced in a different manner. At 12 and 25 μm we see a discrepancy at the low flux levels. The PSC fluxes are consistently higher below 0.4 Jy. The (known) flux overestimate in the PSC at low levels may be the explanation for this effect. At 12 μm the agreement is otherwise quite good, about the 10 % quoted in section 2. For extended sources and for relatively low quality sources in our list or in the PSC we find higher fluxes than in the PSC. At the other wavelength bands the number of such sources increases. The agreement with the high-quality sources is nevertheless very good. In the 60 and 100 μm bands, most sources have higher fluxes than in the PSC. The determination of the background is very important for calculating fluxes in these bands. The PSC filter works in the scan direction, while we compare different two-dimensional maps. It is not known to us how the PSC point source filter has interpreted the extended background structure of the SMC. We estimated the background for each source individually, and we believe that this visual investigation of the maps gives better results in confused regions than automated programs. A comparison of the fluxes of our maps and the IRAS SSS shows that some have very good agreement, but several show a lower flux on the DPM maps.

5. Identification of sources.

5.1 STARS IN THE DPM FIELDS.

5.1.1 *Comparison with SAO stars.* — We have compared the Smithsonian Astrophysical Observatory Star Catalog (1966, henceforth the SAO Catalog) with our source database. Here we searched deeper (to 10^{-8} Watt m^{-2} sr^{-1}) on averaged maps than in the infrared source list (Tab. IV) on the SAO positions. Detection of infrared emission on the known optical position depends on local noise and background (often 3 - 4 times less than the global noise given in Tab. III). The area of the SMC covered by the DPM maps contains 45 SAO stars. We detect 28 of these (mainly at 12 μm) and we have possible detections of five (for positional accuracy, see Sect. 4.2). The remaining 12 stars are below the local map sensitivity limits. In table V we give the relevant data. Columns 1, 2 and 3 are taken from the SAO Catalog (version 1984). Columns 4 and 5 give the colour-corrected 12 and 25 μm flux densities as measured from the DPM maps. The low flux densities are more affected by noise etc. and therefore have higher uncertainties. Column 6 gives the ratio $f_{25\,\mu m}/f_{12\,\mu m}$ together with their uncertainties. If the spectrum of a star follows the Rayleigh-Jeans tail of the blackbody emission this ratio should be about 0.23. The ratio gives information about a possible 25 μm excess relative to 12 μm ($f_{25\,\mu m}/f_{12\,\mu m} > 0.23$). The uncertainties are rather high because of the faint 25 μm emission. Only one star (SAO 255735) may possibly have a 25 μm excess. Column 7 contains the $m_V - m_{12}$ colour, which informs us about a possible 12 μm excess (relative to the optical V band). We compared this column with the $V - [12]$ colours listed in table III of Waters *et al.* (1987) for the range of spectral types (A0 – K5). The stars are scattered within a 1 magnitude band around the values of Waters *et al.* (1987). Most of them have somewhat higher $m_V - m_{12}$ values, but we do not find any star with a significant $m_V - m_{12}$ excess due to the large scatter. The error in $m_V - m_{12}$ is about 1.0 mag. On average these stars have an excess of 0.3 ± 0.2 mag. Column 8 gives the indentification of the SAO star in the infrared source list of table IV. Out of the full sample of SAO stars fourteen can be found in that table (with intensities larger than 3×10^{-8} Watt m^{-2} sr^{-1} at 12 μm). SAO 255752 is detected on the maps, but an optically weaker (non-SAO) star at about 2′ East is brighter in the infrared (LI-SMC 198 in Tab. IV). Column 9 gives the quality of the detection of the star on the infrared maps, and column 10 gives some remarks. Only SAO 255684 shows some possible 60 μm emission. All eight G-type stars and thirteen out of fifteen K-type stars were detected at 12 μm ; four out of six A-type stars and eight out of sixteen F-type stars were detected. There is no clear correlation between detection and visible magnitude in the whole SAO sample. But A-stars have been detected up to $m_V \approx 8.4 \pm 0.5$, F-stars up to $m_V \approx 9.0 \pm 0.6$, G-stars up to 10.0 and K-stars up to 9.1 magnitudes. Emission at 25 μm is detected only from stars later than F5. All stars with 25 μm emission also have 12 μm emission. Most from stars later than F5. All stars with 25 μm emission also have 12 μm emission. Most of these stars are probably Galactic foreground stars.

5.1.2 *Comparison with Radcliffe SMC-stars.* — We also searched for emission from verified SMC stars (Feast *et al.*, 1960) and we detected emission in the direction of eight (out of 46). In the direction of another 18 we found possible weak emission. The Feast SMC stars are on average fainter than SAO stars by 3 or 4 magnitudes (the brightest being R 45 with m_V =10.13). They are the brightest SMC members

(see Azzopardi and Vigneau, 1982). One star, R 10 is within a beam size from SAO 255715, and the emission is caused by the SAO star. R 8 is weakly indicated in the maps. R 14 is close to the HII region N 66 and probably we see emission from N 66 at 12 μm rather than from the star. R 44 is associated with the HII region N 81 (HDE 7113), and we detect this HII region in the infrared. Four other stars (R 28, 29, 31, 32) are close to the Hα nebulosity N 76 so that their detection likewise is not quite certain. More details about the comparison are given in table VI. We conclude that the emission found is due to positional coincidence with other objects, and is not from the SMC stars itself. For twelve Radcliffe stars we mention possible positional infrared identifications in table IV, of which only three have an S-type infrared spectrum. We conclude that these associations are also due to positional coincidences.

Because these stars are the brightest SMC stars we did not continue to look for emission from the whole list of 524 objects of Azzopardi and Vigneau (1982). Using the definition of 12 μm magnitudes (see IRAS, 1985b ; and Tab. III) the IRAS sensitivity limit becomes $m_{12} \approx 6$ mag. Waters *et al.* (1987) give a relation between intrinsic $V - [12]$ colours and spectral type ; for A-type stars $V - [12]$ is about 0 mag and for K-type stars about 2.5 mag. Therefore the weakest A-type stars detectable by IRAS are of a visible magnitude $m_V \approx 6$ mag and K-type stars have $m_V \approx 10$ mag. Because the brightest SMC stars have $m_V \approx 10.1$ mag, only stars with an infrared excess can be detected at a distance of the SMC (63 kpc).

5.1.3 Comparison with Late Type Giants. — A comparison with the list of Carbon and late M-type stars (Blanco *et al.*, 1980) gives one possible detection. LI-SMC 54 (in Tab. IV) is situated 1'.5 West of the position of B 13 in the SMC Bar. This star is one of the list of Blanco *et al.* from which Cohen *et al.* (1981) detected near-infrared emission. The list contains 83 stars in the Bar and 56 in the Wing. Confusion in the SMC Bar may have resulted in this association, but may also be the reason that no others were detected. Another infrared source, LI-SMC 140, is situated 1' NE of the position of an irregular variable star HV 11423 (Payne-Gaposchkin, 1966). Near-infrared emission from this star was detected by Glass (1979). The 12 μm flux density is about ten times higher than the 2.2 mag point of Glass shifted to the longer wavelengths *via* the Rayleigh-Jeans tail of a blackbody spectrum. If the association is correct the reason for this may be its (irregular) variability. HV 11423 is the brightest star in the K-band and is the most luminous M-type variable in the SMC (Glass, 1979).

5.1.4 *Stars : conclusion.* — In table IV there are 43 sources with and S-type infrared spectrum. Of these, fourteen are SAO stars. We looked at the other 29 objects on the photographic ESO-SRC Southern Sky Survey. Eighteen of them can be identified on those plates with stars (probably foreground ; six fairly bright, twelve faint stars). Nine could not be identified because they are in the crowded SW-Bar. Most infrared spectra marked S in table IV (outside the Bar) have an optical identification, but often there is more than one star within a single beam so that these identifications are only tentative. We compared the list of infrared sources with an S-type spectrum with the list of SMC members of Azzopardi and Vigneau (1982). Six objects (infrared sources 19, 48, 96, 106, 107, 186) are within 2' from an SMC member in that list (respectively AZV 2*, 36, 148, 164, 170, 438*). These stars are A and B-type supergiants with $m_V \approx 13$ mag. They are situated in the crowded SMC Bar, and therefore may be misidentified due to confusion. If the association is correct they must have an infrared excess, otherwise they would have stayed invisible at 12 μm. Of the S-type infrared spectra there is one Galactic globular cluster NGC 362, and one SMC globular NGC 419 (Tab. IV ; K 58 in Kron, 1956 ; L 85 in Lindsay, 1958) in our source list (see Sect. 5.3).

5.2 Hα nebulosities in the SMC. — A good overall agreement between Hα emission regions and IRAS infrared emission was already noted by Schwering (1985). In table VII we present a more detailed comparison of the IRAS data with the Hα catalogues of Henize (1956) and of Davies *et al.* (1976, henceforth DEM). The DEM catalogue contains 167 entries ranging in size from 0' to 30'.DEM entries 1 (N 3), 166 (N 90) and 167 are not covered by the IRAS DPM maps ; they are discussed in appendix A. About 70 % of all the bright Hα nebulosities have clear infrared counterparts, 15 % have possible counterparts and the remaining 15 % do not show any clear infrared emission. For the fainter nebulosities the statistics are 50 % detected in the infrared, and 25 % possible detections, while the remaining 25 % does not show any infrared emission. We conclude that there is a higher detection probability in the infrared for the brighter HII regions. We detected infrared emission from about 70 % of the compact Hα knots, while 60 % of the shells were detected.

The whole SMC is covered by Hα nebulosities (see DEM, 1976), and also by 60 and 100 μm infrared radiation. From this comparison, we see that the discrete infrared sources correlate well with HII regions, and that HII regions are one of the main contributors to the infrared radiation in the SMC.

5.3 Clusters in the SMC. — We compared the list of star clusters of Kron (1956), Lindsay (1958) and of Hodge and Wright (1974) with our source list and the infrared maps. The clusters listed in Westerlund and Glaspey (1971) are not covered by the DPM maps. These four lists contain 220 clusters of sizes ranging from a few tenths of an arcminute to a few arcminutes. We searched deeper on the maps than in table IV. In total we have 37 possible infrared detections of clusters, of which 20 have associations in table IV. Sixteen of these infrared sources also have been associated to table VII, showing the confusion with HII regions. Of these 37 possible detections, two are very reliable. They coincide with blue globular clusters ; K 35 (= L 54 = NGC 330) and K 58 (= L 85 = NGC 419) are detected at 12 and 25 μm. These two are the brightest visual SMC globular clusters (van den

Bergh, 1981). The remaining possible infrared associations have mainly 12 μm emission and are very weak. Some are also seen at 60 and 100 μm. Results of this comparison are given in table VIII.

We have also compared the globular clusters or compact groups from the list of 168 new clusters of Brück (1976; her types 1, 2 and 3). Only B 52 is such a cluster. All other new clusters are large loose groups, mainly blue or small blue clusters. There is an infrared source (LI-SMC 59) at about 1′ SE but there is some extended emission present as this position in the SMC-Bar. LI-SMC 59 is also associated to HII region DEM 51 (see Tab. VII), which shows the confusion in the Bar. Recently Hodge (1986) added 213 new clusters in the SMC which brings the total number of cataloged clusters to 601. These new clusters are very small and faint and we do not expect much infrared emission from them.

5.4 SUPERNOVA REMNANTS IN THE SMC. — We checked the list of six supernova remnants of Mathewson *et al.* (1983; their Tab. II). All SNRs are smaller (0′.5 – 5′) than the IRAS beam size at 100 μm. The first three remnants are situated in the crowded SW-Bar of the SMC. SNR 0045-73.4 coincides with extended emission between infrared sources LI-SMC 36 and 43 (see Tab. IV). SNR 0046-73.5 is located close to the edge of source 42, and SNR 0049-73.6 is situated in an infrared hole near sources 68 and 70. The last three are located in the NE part of the Bar. SNR 0101-72.4 can probably be associated with infrared source 160 (at 2′.3 South) at about 6′ from N 76. It is situated on infrared extended emission South of N 76. SNR 0102-72.3 is close to the East of N 76. There is some weak extended emission, but no clear correspondence with the remnant. SNR 0103-72.6 is situated 1′.5 North of the peak of LI-SMC 169. All these associations are already given in table VII of the Hα nebulosities. Table IX summarizes this comparison.

5.5 PLANETARY NEBULAE IN THE SMC. — We compared the DPM infrared maps and the source list with the planetary nebulae identified by Sanduleak *et al.* (1978) and Sanduleak and Pesch (1981). Of their list of 34 nebulae numbers Sk 1, 2, 4, 20 and 29 are not covered by the IRAS DPM observations. The sizes of these nebulae are of order 1″. Many of the nebulae are situated in extended infrared emission in the Bar and in the Wing. Seven nebulae (Sk 5, 6, 11, 15, 17, 19, 27) have probably infrared counterparts, and we have possible detections of six. We give results of the comparison in table X. Again we searched deeper than in table IV. Only four nebulae have associations in table IV. Sk 9 (with infrared LI-SMC 29) is positioned within one beam size of Hα nebulosity N 13, therefore the association is not very reliable. Sk 19 is also close to an Hα structure, but is probably real. A few sources show up in all four wavelength bands.

Nebula Sk 11 is very bright in the infrared. Extrapolating its flux densities using the ratio $f_{60\,\mu m}/f_{100\,\mu m}$ as a temperature measure ($T_d \approx 50$ K) and assuming a dust emissivity with a λ^{-1} wavelength dependence, we find $L_{IR} = 3.7 \times 10^4\ L_\odot$. This is high for a planetary nebula. The luminosity of the star is usually 3 to 10 times higher than the infrared luminosity (Pottasch, 1986). Paczynski's (1971) evolution tracks for planetary nuclei give a stellar luminosity of $5 \times 10^4\ L_\odot$ for the most luminous cases. For the Galactic planetary nebula NGC 6537 the IRAS PSC gives flux densities of 7.7, 58.3, 190 and 166 Jy at 12, 25, 60 and 100 μm. An extrapolation of these IRAS flux densities (with $T_d = 55$ K) gives $L_{IR} = 2300\ L_\odot$ (16 times less). Pottasch (1986) finds for 16 Galactic planetary nebulae values for $L_{IR}/L_\odot$ of typically a few hundred. The extrapolation gives a good estimate of the infrared luminosity for a continuum spectrum. According to Pottasch (1986) line radiation can form a large fraction of the emission from average size nebulae in the IRAS survey bands and may even dominate the continuum in these bands, probably also at 60 and 100 μm (Leene and Pottasch, 1986). If that is the case the infrared luminosity is an overestimate. If we assume a distance of 2.4 kpc for NGC 6537 (Gathier, 1984), a nebula with the same infrared brightness as NGC 6537 would have flux densities of 0.01, 0.08, 0.3 and 0.2 Jy in the IRAS bands at the distance of the SMC. This is about equal to our detection limits. For most identifications other than the brightest (Sk 11) we actually find flux densities of this order (see Tab. X). Four nebulae have their infrared emission peak at 25 or 60 μm, which is typical for planetary nebulae (see e.g. NGC 6537).

5.6 DARK CLOUDS IN THE SMC. — We compared the infrared data with the dark nebulae listed by Hodge (1974). In this paper about the LMC, Hodge (1972) discussed the uncertainties related to incompleteness of his list. These 45 dark clouds range in size from 1′ to 6′. In the comparison we used positions from his Plate-I after we discovered that six nebulae (21, 30, 37, 40, 41, 45) differ from the positions in his table I. Results are listed in table XI. The infrared emission at 60 and 100 μm follows the nebulae in the SW-Bar very well. At the East side of the SW-Bar the infrared follows the dark clouds 29, 30, 32 and 33. All known dark nebulae are in the Bar and the Wing. Nineteen have an association in table IV. Most clouds can be associated with an infrared feature but some (31, 39, 40, 43) are associated with an infrared minimum.

6. Conclusions.

In the SMC DPM maps, 219 discrete sources were found; 143 of these are identified with sources in the IRAS Point Source Catalog (PSC). Sixteen sources correspond to sources in the IRAS Small Scale Structure Catalog (SSS). We found a total of 72 sources not listed in either of these catalogues. In many cases, we determine actual flux densities for sources while the PSC gives only upper limits. Most sources are associated with known HII regions and dark clouds in the SMC. At the positions of known objects in the SMC, we conducted deeper searches of the maps. The results are as follows.

Out of 45 SAO stars, we detected infrared emission from 28, and possibly five more. No cataloged stars in the SMC were identified with certainty, but 29 infrared, non-SAO sources with stellar-type infrared spectra were found, most

of which have possible optical counterparts. One Galactic globular cluster (NGC 362) and two SMC globular clusters (NGC 330 and NGC 419) were also detected. Thirty-five open clusters have possible infrared counterparts. No clear correlation between supernova remnants and infrared emission was found. Infrared emission is seen towards seven, and possibly six more, planetary nebulae (out of 29). However, the majority of these objects is confused with other infrared emitting objects.

Acknowledgements.

We wish to thank the following people : the SDAS team that supported the first reduction stage and assisted PS during his stay at the Jet Propulsion Laboratory ; E. Kopan, P. Alphenaar, A. Vos and D. Hogeweg for writing the necessary software ; Drs. H. Habing, J. Emerson and T. de Jong for scheduling the observations ; Drs H. Habing, W. Rice, R. Walterbos, R. Braun, A. van Genderen and H. Caspers for discussions. PS is grateful for financial support from the Space Research Organisation in the Netherlands (SRON), a subsidiary of the Netherlands Organization for Scientific Research (NWO) during his stay at JPL. We also want to thank the Astronomical Data Center at the NASA Goddard Space Flight Center for providing the SAO Catalog (version 1984) and the library of the Royal Observatory of Edinburgh for a prompt sending of a copy of an Occasional Report.

Appendix A.

Additions to the Infrared Source List.

A.1 Introduction.

This infrared survey at 12, 25, 60 and 100 μm covers the SMC with the exception of the outermost SE and SW parts, containing the HII regions DEM 1 (Davies *et al.*, 1976 ; N 3 in Henize, 1956), DEM 166 (N 90) and the Hα filaments of DEM 167 (see Sect. 5.2). The latter object corresponds to the only known supergiant shell in the SMC (Meaburn, 1980). To complement the maps obtained from the Additional Observations, we derived IRAS (Co-added) maps using Survey data to cover the missing regions. Because these maps are produced from a different database than the DPM derived maps described in this paper, we decide to discuss these maps in an appendix.

A.2 Observations and data reduction.

The maps used in this Appendix are based on Co-added IRAS Survey data, specially produced at Leiden Observatory. We did not use the IRAS 16°.5 Skyflux images (IRAS, 1985a) because of their lower resolution (4′ to 6′). The Co-added Survey data give a resolution that is equal to the resolution of the Additional Observations (see Section 3). Input to the Co-add processor are the Boresight Pointing History File (BPHF) and Calibrated Reconstructed Detector Data (CRDD), calibrated to the May-1984 intermediate standard from the Leiden Observatory IRAS database.

First, we selected all IRAS Survey scans in an area of radius 1° centered on the supergiant shell DEM 167 ($\alpha_{1950} = 01^h28.0^m$, $\delta_{1950} = -73°35'$), and DEM 1 ($\alpha_{1950} = 00^h29.6^m$, $\delta_{1950} = -74°04'.3$). This was done by searching the Zodiacal Observation History File (ZOHF ; IRAS, 1985a). In total 48 scans are covering the field of DEM 167 and 38 are covering the field of DEM 1 ; all these scans were used in the Survey Co-adds. The Zodiacal emission varies smoothly (see Skyflux's HCON-1, HCON-2 and HCON-3), and there is little variation in the infrared emission gradient with time at this high ecliptic latitude ($\beta = -65°$), allowing us to add all data from the three HCONs. Most scans have equal scan position angles to within 20°. The average scan position angle (NESW) in the field of DEM 167 is 107° and in the field of DEM 1 119°. In the first field there are 6 scans with very different scan angles (about 158°), while in the latter field only one scan has a clearly different scan position angle (42°). The search radius of 1° was chosen to obtain overlap between the DPM and Co-added maps so as to be able to compare the SMC extended emission and to compare discrete sources in two independent map sets. The scan length selected from the CRDD is 32 seconds (at a scan rate of 3′.85/sec) enough to cover a 2° field.

The IRAS Survey scans were gridded onto a map of 2° × 2° centered on DEM 167, respectively DEM 1, by using the same software (DSCO, DSGAD) as described in section 2. The scans were added in the order of increasing distance from the field centre in order to have as much overlap in the scan-maps as possible in all subsequent additions. This overlap is important in identifying a better median offset to adjust individual scan-maps to the same intensity level. Because of the inclusion of HCON-3 scans (SOP > 425 ; 30 % of all scans) the median noise dropped by a factor of 2 relative to individual scan-maps. To bring the calibration to the November-1984 calibration of IRAS (IRAS, 1985a ; final product), we applied multiplication factor of 0.97, 0.98, 0.93 and 0.74 in the 12, 25, 60 and 100 μm bands (Kopan, priv. comm.). These factors were checked againt the behaviour of the eight IRAS calibration stars (see IRAS, 1985a), and NGC 6543 in a set of calibration Co-adds (Caspers, priv. comm.). As the low level contours from the Co-added and the DPM maps connect very well, we did not attempt to further improve on the background correction.

A.3 The maps of infrared radiation.

The 12 μm maps show some resulting stripes of 1′ wide and 12′ apart caused by the smaller edge detectors (see IRAS, 1985a). Special care was taken in the interpretation of positions affected by this artifact. These effects are not present in the other wavelength maps. Due to an error in the search for IRAS Survey scans, those covering only the outer edges were not accepted resulting in an increased noise at the NE and SW edges ($\sim 10'$) of the field centered on DEM 167, and noisy and not-covered NE and SW edges of the same size in the field centered on DEM 1. Further characteristics of the Co-added maps are given in table A.1. These maps are presented in Schwering and Israel (1989).

Comparing table A.1 with table III we note that the noise is about two times less at 12 and 25 μm and four times less at

60 and 100 μm compared to the AOs. This can be explained by the higher number of coverages (roughly ten for the Co-adds and about five for each AO set), but mainly by the lower amount of extended emission in the maps (especially at 60 and 10 μm). The zero-level is more uncertain (about five times), because no plane was fitted to the maps, but only an offset was subtracted. The stripe residuals are about the same.

In the 12 and 25 μm maps some Zodiacal foreground emission is present in the form of a background slope in the maps of both fields with higher levels at the NW (about $+10^{-8}$ Watt m^{-2} sr^{-1}) and lower at the SE edges (-10^{-8} Watt m^{-2} sr^{-1}). In the 60 and 100 μm maps variations in the fields are caused by the extended emission of the SMC itself. No variation due to the Galactic foreground cirrus can be seen in these maps.

A.4 Additions to the Infrared Source List in the SMC.

We have searched these maps in the same way as the DPM-maps in section 4. Note that we have only a single map of these two fields in contrast to the three independent DPM-maps. Table A.2 contains the additions to the source list table IV.

We checked all sources from the DPM-maps (Tab. IV) and all sources from the IRAS PSC (IRAS, 1985a) and the IRAS SSS (IRAS 1985b). The IRAS PSC and SSS are based on the same data that were used in preparing the Co-added maps in this Appendix. All IRAS PSC entries in these two fields were confirmed by us, and are included in our source list. For all IRAS SSS sources infrared counterparts were found on the maps. In total we found thirty additional infrared sources in these fields of which fifteen are related to the IRAS PSC and SSS catalogs. Thus fifteen new infrared sources were found.

A.5 Identification of sources.

In this Appendix we are primarily concerned with the identification of all sources that were not already present in the DPM-maps (i.e. the area with $\alpha > 01^h25^m$ or with $\alpha < 00^h31^m$). For the identification of known objects we searched deeper than the infrared source list of table A.2. None of the known supernova remnants (Mathewson *et al.*, 1983) nor any of the known dark clouds (Hodge, 1974) in the SMC are present in these areas.

A.5.1 STARS IN THE FIELDS.

A.5.1.1 *Comparison with SAO stars.* — In table A.3 we list the seven stars from the SAO Catalog (1966) are present in these areas in the Co-added fields and their colour-corrected 12 and 25 μm flux densities. None of these stars showed emission at 60 or 100 μm.

A.5.1.2 *Comparison with Radcliffe SMC-stars.* — Radcliffe stars (Feast *et al.*, 1960) R 47, 48, 49, which are positioned in the field of DEM 167, show no evidence for infrared radiation coming from these SMC stars. The other field does not contain Radcliffe stars that were not already discussed in section 5.1.2.

A.5.2 Hα NEBULOSITIES IN THE SMC. — The main reason for Co-adding the IRAS Survey data was the failure of the IRAS DPM maps to cover the outermost edges of the SMC, especially HII regions DEM 1 (Davies *et al.*, 1976 ; N 3 in Henize, 1956), DEM 166 (N 90) and 167. The ring of diffuse filaments DEM 167 forms the only SMC supergiant shell, discovered by Meaburn (1980). The bright HII regions DEM 1 (infrared LI-SMC 239) and DEM 166 (LI-SMC 242) are both detected in the infrared. N 1 of Henize corresponds to infrared source number 229. One field is centered on the supergiant Hα shell DEM 167, with a diameter of 32′. In the infrared shell-like filaments are visible at 25, 60 and especially at 100 μm with its centre at $1^h28.4^m, -73°38'$ and a diameter of 24′. The infrared emission follows the Hα quite well except in the North, where the infrared is about 8′ South of the Hα filaments. Infrared sources LI-SMC 240, 241, 245 and 246 are related to this supergiant shell.

A.5.3 CLUSTERS IN THE SMC. — The area of interest to this Appendix in the DEM 167 field, contains no clusters from the list of Kron (1956), four (L 105, 107, 109, 110) from the list of Lindsay (1958), one (WG 1) from Westerlund and Glaspey (1971) and one (HW 86) from Hodge and Wright (1974). Only cluster L 105 shows possible infrared radiation ; it coincides with LI-SMC 242 in the infrared source list (see Tab. A.2). Confusion with the Hα nebulosity DEM 166 makes this identification uncertain ; the infrared source is probably related to the HII region and not to the cluster. L 107 in positioned in extended emission of DEM 167.

The area of interest in the DEM 1 field, contains seven Kron clusters (K 1, 4, 5, 6, 8, 9, 10), eight Lindsay clusters (L 3, 4, 6, 7, 9, 12, 13, 15 ; the last seven are the same as the Kron clusters listed here) and three (HW 2, 3, 4) Hodge and Wright clusters. Of these only K 6 (= L 9) possibly shows weak infrared at 12 μm only (0.15 Jy).

A.5.4 PLANETARY NEBULAE IN THE SMC.— The field of DEM 167 contains no planetary nebulae of the list of Sanduleak *et al.* (1978) and Sanduleak and Pesch (1981), that were not already discussed in section 5.5. In the field of DEM 1 there are two planetary nebulae (Sk 1 and 29) which are in the area of interest. Sk 1 corresponds in position to our source with LI-SMC 229 (in Tab. A.2) and to the Hα object N 1. This source peaks at 25 μm with 0.2 Jy, and there is some possible weak 12 μm emission ($\sim$ 0.15 Jy). Sk 29 was not detected on the maps.

A.6 Conclusions.

In this Appendix we discuss sources on the infrared maps at 12, 25, 60 and 100 μm of the outermost SE and SW corners of the Small Magellanic Cloud. We found 30 infrared sources, which brings the total of infrared sources in and around the SMC to 249. In the areas that were searched all IRAS Point Sources (PSC) were detected and all IRAS Small Scale Structure (SSS) entries have related infrared sources. Fifteen sources are new detections. We identified the infrared sources where possible. Three

foreground SAO stars were detected in these fields ; no Radcliffe SMC-stars yielded a detection. Hα nebulosities DEM 1, 166 and 167 (a supergiant shell) were all detected in the infrared. The cluster K 6 (L 9), and the planetary nebula Sk (N 1) are possible detections.

References

AARONSON M., MOULD J. : 1982, *Astrophys. J. Suppl. Ser.* **48**, 161.
VAN ALBADA G. D., BAUD B., DE PAGTER P. J., POL W., RENES J. J., WESSELIUS, P. R. : 1985, ROG Internal Report.
ALLEN D. A., GLASS I. S. : 1976, *Astrophys. J.* **210**, 666.
AZZOPARDI M., VIGNEAU J. : 1982, *Astron. Astrophys.* **50**, 291.
VAN DEN BERGH S. : 1981, *Astron. Astrophys. Suppl. Ser.* **46**, 79.
BLANCO V. M., MCCARTHY M. F., BLANCO B. M. : 1980, *Astrophys. J.* **242**, 938.
BURTON W. B., DEUL E. R., WALKER H. J., JONGENEELEN A. A. W. : 1986, Light on Dark Matter Ed. F. P. Israel (Reidel Dordrecht) 357.
BRÜCK, M. T. : 1976, Occ. Rep. R. Obs. Edinburgh 1.
CATCHPOLE R. M., FEAST M. W. : 1981, *Mon. Not. R. Astron. Soc.* **197**, 385.
COHEN J. G., FROGEL J. A., PERSSON S. E., ELIAS J. H. : 1981, *Astrophys. J.* **249**, 481.
DAVIES R. D., ELLIOTT K. H., MEABURN J. : 1976, *Mem. R. Astron. Soc.* **81**, 89.
EPCHTEIN N., BRAZ M. A., SEVRE F. : 1984, *Astron. Astrophys.* **148**, 263.
FEAST M. W., THACKERAY A. D., WESSELINK A. J. : 1960, *Mon. Not. R. Astron. Soc.* **121**, 337.
FEAST M. W., CATCHPOLE, R. M., CARTER B. S., ROBERTS G. : 1980, *Mon. Not. R. Astron. Soc.* **193**, 377.
FEAST M W., WHITELOCK P. A. : 1984, *Observatory* **104**, 193.
FROGEL J. A., COHEN J. C. : 1982, *Astrophys. J.* **253**, 580.
GATHIER R. : 1984, Ph.D. Thesis, University of Groningen.
GATLEY I., BECKLIN E. E., HYLAND A. R., JONES J. J. : 1981, *Mon. Not. R. Astron. Soc.* **197**, 17P.
GATLEY I., HYLAND A. R., JONES J. J. : 1982, *Mon. Not. R. Astron. Soc.* **200**, 521.
GLASS I. S. : 1974, *Mon. Not. R. Astron. Soc.* **168**, 249.
GLASS I. S. : 1979, *Mon. Not. R. Astron. Soc.* **186**, 317.
GLASS I. S. : 1984, *Mon. Not. R. Astron. Soc.* **209**, 759.
GRASDALEN G. L., JOYCE R. R. : 1976, *Astron. Astrophys.* **50**, 297.
HENIZE K. G. : 1956, *Astrophys. J. Suppl.* **2**, 315.
HODGE P. W., WRIGHT F. W. : 1974, *Astron. J.* **79**, 858.
HODGE P. W. : 1972, *Publ. Astron. Soc. Pac.* **84**, 365.
HODGE P. W. : 1974, *Publ. Astron. Soc. Pac.* **86**, 263.
HODGE P. W. : 1986, *Publ. Astron. Soc. Pac.* **98**, 1113.
HUMPHREYS R. M. : 1984, Structure and Evolution of the Magellanic Clouds, IAU Symp. 108, Eds. S. van den Bergh, K. S. de Boer (Reidel Dordrecht) 145.
IRAS : 1985a, IRAS Catalogs and Atlases Explanatory Supplement, Eds. C. A. Beichmann, G. Neugebauer, H. J. Habing, P. E. Clegg, T. J. Chester, JPL D-1855.
IRAS : 1985b, IRAS Small Scale Structure Catalog, Eds. G. Helou, D. W. Walker, JPL D-2988.
IRAS : 1986, A guide to IRAS pointed observation products, Eds. E. T. Young, G. Neugebauer, E. L. Kopan, R. D. Benson, T. P. Conrow, W. L. Rice, D. T. Gregorich, G. K. Miley, IPAC preprint PRE-008N.
ISRAEL F. P. : 1984, Structure and Evolution of the Magellanic Clouds, IAU Symp. 108, Eds. S. van den Bergh, K. S. de Boer (Reidel Dordrecht) 319.
ISRAEL F. P., KOORNNEEF J. : 1988, *Astron. Astrophys.* **190**, 21.
ISRAEL F. P., KOORNNEEF J., SCHWERING P. B. W. : 1989, in preparation.
ISRAEL F. P., SCHWERING P. B. W. : 1986, Light on Dark Matter, Ed. F. P. Israel (Reidel Dordrecht) 383.
JONES T J., HYLAND A. R., STRAW S., HARVEY P. M., WILKING B. A., JOY M., GATLEY I., THOMAS J. A. : 1986, *Mon. Not. R. Astron. Soc.* **219**, 603.
KOORNNEEF J., ISRAEL F. P. : 1985, *Astrophys. J.* **291**, 156.
KOPAN E. L. : 1982, IRAS/SDAS Subsystem Design Specification 623-75 : Deep Sky Survey Subsystem Rev. A, Jet Propulsion Laboratory, California Institute of Technology, Pasadena California.
KOPAN E. L. : 1984, Interoffice memorandum 84-SDAS-241, Jet Propulsion Laboratory, Pasadena California.
KRON G. E. : 1956, *Publ. Astron. Soc. Pac.* **68**, 125.
LEENE A., POTTASCH S. R. : 1986, Light on Dark Matter, Ed. F. P. Israel, Reidel Dordrecht, 143.
LINDSAY E. M. : 1958, *Mon. Not. R. Astron. Soc.* **118**, 172.
LINDSAY E. M. 1961, *Astron. J.* **66**, 169.
MATHEWSON D. S., FORD V. L., DOPITA M. A., TUOHY I. R., LONG K. S., HELFAND D. J. : 1983, *Astrophys. J. Suppl.* **51**, 345.
MEABURN J. : 1980, *Mon. Not. R. Astron. Soc.* **192**, 365.

MOULD J., AARONSON M. : 1980, *Astrophys. J.* **240**, 464.
MOULD J., AARONSON M. : 1982, *Astrophys. J.* **263**, 629.
PACZYNSKI B. : 1971, *Acta Astronomica* **21**, 417.
PAYNE-GAPOSCHKIN, C. H., GAPOSCHKIN S. : 1966, Smithsonian Contr. Astrophys. 9.
PERSSON S. E., AARONSON M., COHEN J. G., FROGEL J. A. : 1983, *Astrophys. J.* **266**, 105.
POTTASCH S. R. : 1986, Light on Dark Matter, Ed. F. P. Israel (Reidel Dordrecht) 131.
PRICE S. D., WALKER R. G. : 1976, The AFGL Four Color Infrared Sky Survey : Catalog of Observations at 4.2, 11.0, 19.8 and 27.4 μm, AFGL-TR-76-0208, Hanscom Air Force Base, Massachusetts : Air Force Geophysics Laboratory.
RUSSEL S. E., HYLAND A. R. : 1985, *Proc. Astron. Soc. Aust.* **6**, 52.
SANDULEAK S. N., MACDONNELL D. J., DAVIS PHILIP, A. G. : 1978, *Publ. Astron. Soc. Pac.* **90**, 621.
SANDULEAK N., PESCH P. : 1981, *Publ. Astron. Soc. Pac.* **93**, 431.
SCHWERING P. B. W. : 1985, New Aspects of Galaxy Photometry, *Lect. notes Phys.* **32**, Ed. J. L. Nieto (Springer Verlag Berlin) 115.
SCHWERING P. B. W., ISRAEL F. P. : 1989, Atlas and Catalogue of IRAS far-infrared observations of the Magellanic Clouds, in preparation.
Smithsonian Astrophysical Observatory Star Catalog (4 vols.) : 1966, Waschington D.C., Smithsonian Institution (version 1984).
WATERS L. B. F. M., COTE J., AUMANN H. H. : 1987, *Astron. Astrophys.* **172**, 225.
WELCH D. L., MADORE B. F. : 1984, Structure and Evolution of the Magellanic Clouds, IAU Symp. 108 Eds. S van den Bergh, K. S. de Boer (Reidel, Dordrecht) 221.
WESTERLUND B. E., GLASPEY J. : 1971, *Astron. Astrophys.* **10**, 1.
WERNER M. W., BECKLIN E. E., GATLEY I., ELLIS M. J., HYLAND A. R., ROBINSON G., THOMAS J. A. : 1978, *Mon. Not. R. Astron. Soc.* **184**, 365.

TABLE I. — *Other infrared observations of the Magellanic Clouds* ([a, b]).

Spectral range	Reference	Number of Objects SMC	LMC	Objects
Near-infrared photometry ($\lambda < 30$ μm):				
	Grasdalen and Joyce (1976)	6	0	N9,N13A,N25,N46, N64A,N81
	Price and Walker (1976) [c]	0	4	30 Dor,N159 (2 more)
	Gatley *et al.* (1981)	0	1	N159
	Gatley *et al.* (1982)	1	0	N76B
	Epchtein *et al.* (1984)	2	2	N160A,N105A
	Koornneef and Israel (1985)	1	0	N81
	Jones *et al.* (1986)	0	5	N10,N59A,N158C, N160,N159
	Israel *et al.* (1988)	9	16	Various sources
Near-infrared spectro-photometry ($\lambda < 5$ μm):				
	Koornneef and Israel (1985)	1	0	N81
	Israel and Koornneef (1988)	3	6	N81,N85,N88 (SMC); N7,N83B,N11A,N213A, 30 Dor,N159 (LMC)
Far-infrared photometry($\lambda > 30$ μm) [c]:				
	Werner *et al.* (1978)	0	4	30 Dor,N158, N160A,N159
	Jones *et al.* (1986)	0	4	N159,N160A,N59A,N158

Notes to Table 1:

a) Near-infrared stellar surveys are excluded: Glass (1974), Allen and Glass (1976), Glass (1979), Feast et al. (1980), Catchpole and Feast (1981), Cohen et al. (1981), Feast and Whitelock (1984), Glass (1984), Welch and Madore (1984), Russel and Hyland (1985).

b) Near-infrared surveys of cluster stars and integrated cluster photometry are excluded: Mould and Aaronson (1980), Aaronson and Mould (1982), Mould and Aaronson (1982), Frogel and Cohen (1982), Persson et al. (1983).

c) The observations of Price and Walker (1976) were done with a rocket experiment; the far-infrared observations were obtained with NASA's Kuiper Airborne Observatory. The other observations in this table are all ground based.

TABLE II. — *IRAS DPM Observations of the SMC.*

(1) IPAC[a] grid number	(2) SOP-OBS[a]	(3) Observation Id	(4) Grid centre position[b] RA(1950) h m s	DEC(1950) ° ' "	(5) Pos.Ang[c] (NESM) Deg	(6) Map/Obs[d] set
11192	475-049	CG2023-01[e]	00 42 33	-74 00 47	255.7	3 EM
11123	473-045	CG2023-00	00 42 34	-74 00 54	254.7	3 EM
11152	474-024	CG2022-00	00 43 49	-72 32 25	254.6	3 EM
11440	484-010	CG2022-01	00 45 24	-72 29 19	258.8	3 EM
06006	339-012	CG1676-03	00 45 42	-73 58 49	184.3	2 NS
05694	321-007	CG1676-02	00 45 56	-73 57 29	175.1	2 NS
05699	321-018	CG1676-03	00 45 56	-73 57 31	175.2	----
05645	319-029	CG1676-00	00 45 56	-73 57 13	174.3	2 NS
05648	319-036	CG1676-01	00 45 56	-73 57 17	174.4	2 NS
05851	329-012	CG1750-00	00 46 55	-73 58 08	179.0	----
04915	293-010	CG1459-01	00 47 02	-73 56 16	161.1	1 NS
04870	290-030	CG1459-00	00 47 04	-73 56 03	159.9	----
05188	309-020	CG1459-01	00 47 05	-73 57 04	168.9	1 NS
05830	327-024	CG1675-02	00 47 47	-72 29 03	177.3	2 NS
05635	319-003	CG1675-02	00 47 48	-72 28 25	173.0	2 NS
05632	318-042	CG1675-01	00 47 48	-72 28 23	172.9	2 NS
05640	319-009	CG1675-03	00 47 48	-72 28 24	173.0	2 NS
05594	318-005	CG1675-00	00 47 48	-72 28 24	172.5	----
04820	288-036	CG1458-01	00 47 55	-72 27 00	158.3	1 NS
04755	287-016	CG1458-00	00 47 57	-72 26 52	157.5	1 NS
11218	476-028	CG2024-00	01 04 22	-72 30 11	250.2	3 EM
11257	478-004	CG2024-01	01 04 22	-72 30 07	250.9	3 EM
11129	473-052	CG2025-00	01 04 44	-73 59 03	249.0	3 EM
11211	476-022	CG2025-01	01 04 48	-73 58 57	250.2	3 EM
05907	333-028	CG1677-01	01 07 44	-72 26 25	175.6	----
05872	330-033	CG1751-00	01 07 49	-72 26 22	174.2	----
05875	331-004	CG1677-00	01 07 50	-72 26 39	174.3	2 NS
05560	317-025	CG1677-02	01 07 52	-72 26 13	167.5	2 NS
05587	317-054	CG1677-03	01 07 55	-72 26 07	167.8	----
05078	303-015	CG1460-01	01 07 57	-72 25 07	160.6	1 NS
04885	291-023	CG1460-01	01 07 58	-72 24 34	154.9	1 NS
04823	289-003	CG1460-00	01 07 59	-72 24 39	153.8	----
05245	311-006	CG1460-01	01 07 59	-72 25 15	164.3	----
05557	317-011	CG1677-01	01 08 00	-72 26 39	167.3	2 NS
05550	317-004	CG1677-00	01 08 00	-72 26 38	167.2	2 NS
05687	320-037	CG1678-02	01 08 57	-73 53 52	169.4	2 NS
05693	321-002	CG1678-03	01 08 57	-73 53 50	169.6	2 NS
05631	318-036	CG1678-00	01 08 58	-73 53 49	168.4	2 NS
05653	319-042	CG1678-01	01 08 58	-73 53 46	169.0	2 NS
04908	292-030	CG1461-01	01 09 05	-73 52 17	155.8	1 NS
04826	289-010	CG1461-00	01 09 08	-73 52 09	154.0	1 NS

Notes to Table 2:
a) For a description of names and abbreviations (Grid, SOP, OBS) we refer to IRAS (1985a) and IRAS (1986).
b) The field size of each observation is 3 degrees in the scan direction and 2 degrees in the cross-scan direction.
c) The scan direction is given by its position angle Pos.Ang (degrees NESM).
d) Map/Obs set 1 and 2 are scanned in the North-South direction, while Map/Obs set 3 is scanned East-West. The number of the set is identical to the number of the combined map in the text (see Section 2 and 3). A dash in this column indicates that the grid was not used in the processing for various reasons. In Figures 2, 3 and 4 we display all three Obs/Map sets.
e) Observation Id CG stands for Close Galaxies.

TABLE III. — *Description of the SMC DPM-map characteristics.*

Characteristic (Unit)	Wavelength band 12 μm	25 μm	60 μm	100 μm
Effective frequency (10^{12} Hz)	25	12	5	3
Bandwidth (μm)	7.0	11.2	32.5	31.5
Bandwidth correction (10^{12} Hz) a)	13.48	5.16	2.58	1.00
Zero-magnitude flux density f_ν (0.0 mag) (Jy)	28.3	6.73	1.19	0.43
Point Source Conversion factor (Jy / 10^{-8} Watt m^{-2} sr^{-1})	0.037	0.11	0.41	2.08
Positional accuracy (″)	15	15	15	15
Nominal detector size(′x′)	0.75 x 4.5	0.75 x 4.7	1.5 x 4.8	3.0 x 5.0
Resolution (′x′) b)	0.9 x 6.4	1.1 x 6.4	2.0 x 6.4	3.8 x 6.4
Absolute calibration (%)	10	10	10	10
Median noise (MJy/sr) c)	0.096	0.097	0.12	0.20
(10^{-8} Watt m^{-2} sr^{-1})	1.3	0.5	0.3	0.2
Zero-level uncertainty (MJy/sr)	0.015	0.019	0.039	0.10
(10^{-8} Watt m^{-2} sr^{-1})	0.2	0.1	0.1	0.1
Stripe residuals (MJy/sr) d)	0.052	0.058	0.12	0.30
(10^{-8} Watt m^{-2} sr^{-1})	0.7	0.3	0.3	0.3
Sensitivity (MJy/sr) e)	0.3	0.3	0.4	0.6
(10^{-8} Watt m^{-2} sr^{-1})	4	2	1	0.5

Notes to Table 3:
a) Chester (priv. comm.).
b) The Gaussian resolution is given in arc-minutes (in-scan x cross-scan). One arcminute at the distance of the SMC (63 kpc) corresponds to 18.pc.
c) The value of the median noise is influenced somewhat by the extended emission of the SMC itself. The real detector noise is somewhat lower.
d) Higher stripe levels than the average level given in the table can occur.
e) The sensitivity indicates the intensity limits of Table 4. Note that the IRAS PSC sensitivity limits are 0.25, 0.25, 0.40, 1.00 Jy (see IRAS, 1985a).

TABLE IV. — *Infrared Source List in the SMC.*

(1)	(2)		(3)		(4)		(5)		(6)		(7)	(8)	(9)	(10)	(11)	(12)	(13)	(14)
Number	Position		12 μm		25 μm		60 μm		100 μm		Size	F	F	F	F	IRAS-Id	Spec-	Comments
	RA(1950)	DEC(1950)	Peak	Bg	Peak	Bg	Peak	Bg	Peak	Bg		12μm	25μm	60um	100μm		trum	
	h m s	° ′ ″			10^{-6} Watt $m^{-2}sr^{-1}$						arcmin	Jy	Jy	Jy	Jy			
1	00 33 04.3	-73 25 06	-	-	-	-	1	-	1	-	4x9	-	-	1.9	5.7	00330-7325 X0032-734	C	
2	00 33 43.2	-73 37 49	2	-	4	-	3	-	1	0.5	p	0 07	0 44	0.8	1.0	00337-7337	C	
3	00 33 47.8	-74 09 09	23	-	2	-	-	-	-	-	p	0 85	0 22	-	C	00337-7409	S	SAO 255684
4	00 34 04.0	-73 08 03	12	-	-	-	-	-	-	-	p	0.44	-	-	-	00340-7308	S	SAO 255686
5	00 35 04.2	-74 36 17	8	-	2	-	-	-	-	-	p	0.30	0.22	-	-	00350-7436	S	
6	00 35 10.5	-73 16 19	-	-	1	-	4	1	2	1	4x2	-	0.36:	2.5	3.0	00351-7316	C	
7	00 36 24	-74 14	3	-	-	-	-	-	-	-	-	0 11:	-	-	-		S	SAO 255689
8	00 36 44	-73 25	3	-	-	-	<3	-	-	-	-	0 11.	-	-	C		S	SAO 255690
9	00 37 46.8	-73 18 55	-	-	-	-	4	2	4	2	-	-	-	0.8	4.2	00377-7318	C	
10	00 38 55.4	-73 53 40	-	-	-	-	2	1	2	1	-	-	-	0.4	2.1	00389-7353	C	
11	00 39 33.5	-73 17 35	-	-	1	-	8	4	-	-	p	-	0.11	1.7	C	00395-7317	H	
12	00 39 33.7	-74 03 45	-	-	2	-	1	-	-	-	-	-	0.22:	0.4:	C	00395-7403	H	
13	00 40 00	-73 58	5	-	-	-	<2	-	-	-	-	0 19	-	-	C		S	
14	00 40 16.3	-73 47 27	-	-	2	-	7	4	4	3	p	-	0 22	1.2	2.1	00402-7347	C	
15	00 40 20.7	-73 16 28	-	-	2	-	13	6	9	6	p	-	0 22	2 9	6.3	00403-7316	C	
16	00 40 25.8	-74 00 47	-	-	-	-	5	2	2	1	p:	-	-	1.2	2.1	00404-7400	C	
17	00 40 39.3	-74 45 25	-	-	-	-	3	-	1	0 3	p	-	-	1.2	1.5	00406-7445	C	
18	00 40 42	-73 31	-	-	-	-	11	6	10	5	-	-	-	2.1	10.0		C	
19	00 41 01.0	-73 39 45	3	-	-	-	-	-	-	-	-	0.11:	-	C	C	00410-7339	S	
20	00 41 10.0	-73 36 35	3	-	-	-	-	-	-	-	-	0.11:	-	C	C	00411-7336	S	
21	00 41 20.6	-73 16 38	3	-	6	-	18	6	12	5	px1	0.14:	0.80	5.3	15.0	00413-7316 X0040-732	C	
22	00 41 45.2	-74 00 29	12	-	-	-	-	-	-	-	p	0.44	-	C	C	00417-7400	S	
23	00 41 46.3	-73 18 34	3	-	2	-	14	11	-	-	p	0.11:	0.22	1.2	C	00417-7318	H	
24	00 42 51.1	-74 17 36	-	-	-	-	2	-	2	0.5	14x14	-	-	14 0	11.0	00428-7417	H	
25	00 42 59.9	-73 13 58	-	-	6	-	13	9	-	-	p	-	0.67	1.7	C	00429-7313	H	
26	00 43 05.7	-73 26 45	15	4	30	5	60	20	-	-	p	0.41	3.00	17.0	C	00430-7326	H	
27	00 43 13.8	-73 32 52	12	5	15	3	72	20	46	22	p	0.20	1.33	21.0	50.0	00432-7332	C	
28	00 43 30	-73 29	14	6	9	5	72	30	45	22	p	0.30	0 44	17 0	48.0:		C	
29	00 43 32 2	-73 39 10	22	5	21	4	88	20	48	22	p:	0.63	1.89	28.0	54.0	00435-7339	C	
30	00 43 37.1	-73 21 32	9	3	10	2	55	20	35	22	p:	0.22	0.89	14.0	27.0	00436-7321	C	
31	00 43 47 1	-73 34 33	9	6	6	4	-	-	-	-	-	0.11	0.22	C	C	00437-7334	H	
32	00 43 51	-73 39	17	6	6	4	-	-	-	-	p.	0 33	0 22	C	C		S	
33	00 44 32	-72 52	11	-	-	-	<3	-	<4	-	p.	0 41	-	-	-		S	
34	00 44 36	-74 08	9	-	-	-	<2	-	-	-	p	0.33.	-	-	C		S	
35	00 44 38.5	-73 39 02	13	5	12	4	65	30	42	22	1x2	0 60	1.60	19.0	46.0	00446-7339	C	
36	00 44 47.0	-73 22 29	20	6	21	5	100	50	60	40	p	0.52	1.78	21.0	42.0	00447-7322	C	
37	00 44 51	-73 44	9	3	4	2	25	20	-	-	-	0.22	0.22	2.1	C		H	
38	00 44 55.0	-73 47 35	7	-	8	1	36	12	23	10	1x2	0 51	1 40	13.0	30.0	00449-7347	C	
39	00 45 09	-73 39	13	4	6	3	-	-	-	-	2xp:	0.57	0.53	C	C		S	
40	00 45 36	-72 57	8	-	-	-	<3	-	<4	-	p.	0.30	-	-	C		S	
41	00 45 38.1	-73 54 38	5	-	-	-	8	6	-	-	-	0.19:	-	0.8:	C	00456-7354	H	
42	00 46 00	-73 34	21	7	28	7	125	100	-	-	px1	0.64	2.79	11.0	C	X0045-735	H	
43	00 46 12	-73 24	15	10	15	11	125	100	70	60	p:	0.19	0.44	10.0	21.0		C	
44	00 46 15.6	-73 39 56	3	-	2	1	35	25	-	-	-	0 11:	0 11:	4 1	C	00462-7339	H	
45	00 46 17 3	-73 31 37	34	5	95	7	160	25	83	22	p	1 07	0.77	56.0	128.0	00462-7331	C	
46	00 46 21 7	-73 52 11	-	-	-	-	9	7	-	-	-	-	-	0 8	C	00463-7352	H	
47	00 46 23.8	-72 38 22	-	-	-	-	13	5	9	4	5x4	-	-	10.0	20.0	00463-7238	C	
48	00 46 34	-73 01	5	-	1	-	-	-	-	-	-	0.19	0.11:	C	C			
49	00 46 37 6	-73 22 10	23	5	33	8	155	30	93	22	p	0.67	2.78	52.0	149.0	00466-7322 X0046-733	C	
50	00 46 47.2	-73 14 30	5	-	11	2	36	25	27	25	p	0.19	1.00	4.5	4.2	00467-7314	H	
51	00 46 54	-73 26	14	5	20	8	100	50	63	45	p:	0.33	1.33	21.0	38.0	00472-7325	C	
52	00 47 06	-73 43	3	-	7	2	20	15	-	-	p:	0 11:	0.56	2.1:	C	00469-7341:	H	
53	00 47 26.1	-73 50 07	3	-	1	-	9	8	-	-	-	0.11:	0.11:	0.4.	C	00474-7350	H	
54	00 47 26.9	-73 30 45	8	3	-	-	-	-	-	-	-	0.19:	C	C	C	00474-7330	S	
55	00 47 30	-73 27	5	-	12	5	55	30	-	-	p	0.19:	0.78	10.0	C	00477-7328:	H	
56	00 47 37	-73 45	12	-	-	-	-	-	-	-	p	0.44	-	C	C		S	SAO 255711
57	00 47 42.8	-73 43 04	5	-	12	2	50	16	25	12	p	0.19	1.11	14.0	27.0	00477-7343	C	
58	00 47 53.2	-73 05 08	5	-	13	2	50	30	-	-	p	0.19	1.22	8.3	C	00478-7305	H	
59	00 47 57	-73 19	5	-	3	2	36	30	-	-	-	0.19:	0.11:	2.5	C		H	
60	00 48 03	-72 25	5	-	-	-	<3	-	<3	-	-	0.19:	-	-	-		S	
61	00 48 22 1	-73 47 48	17	-	5	1	10	8	-	-	1xp	0.78	0.53	0.9:	C	00483-7347	H:	
62	00 48 23.9	-72 50 11	-	-	2	-	21	9	13	7	3x4	-	0.87:	12.0	19.0	00483-7250	C	
63	00 48 25	-73 09	5	-	10	7	88	25	43	18	3x4	0.83	1.31	61.0	80.0		C	
64	00 48 39 5	-72 37 39	3	-	-	-	10	6	6	4	p	0.11:	-	1 7	4.2	00486-7237	C	
65	00 48 45	-73 08	16	4	14	6	70	25	-	-	p	0.44	0.89	19.0	C	X0048-731	H	
66	00 48 57 5	-73 02 59	5	-	13	3	40	30	-	-	p	0.19:	1.11	4.1	C	00489-7302	H	
67	00 48 59.8	-72 35 48	-	-	-	-	11	9	7	4	2xp	-	-	1.0	6.8	00489-7235	C	
68	00 49 00.0	-73 36 26	-	-	3	2	24	18	16	14	1x1	-	0.15:	2.8	4.3	00489-7336	C	
69	00 49 00.3	-71 25 36	3	-	-	-	-	-	-	-	-	0 11:	-	-	-	00490-7125	S	SAO 255713
70	00 49 07.3	-73 40 54	3	-	4	2	22	17	16	15	p.	0.11:	0.22	2.1	2.1	00491-7340	H	
71	00 49 07.4	-72 46 43	-	-	2	-	15	11	10	8	1x2	-	0.40	2.2	4.6	00491-7246	C	
72	00 49 18	-73 27	5	-	4	2	-	-	-	-	-	0.19	0.22	C	C		H	
73	00 49 28.5	-73 47 29	3	-	2	-	20	15	16	12	p	0.11:	0.22	2.1	8.4	00494-7347	C	
74	00 49 30	-73 00	5	-	3	1	-	-	-	-	p	0.19	0.22:	C	C		H.	
75	00 49 35.7	-72 16 23	-	-	-	-	7	3	6	3	4x5	-	-	5.0	12.0	00495-7216	C	
76	00 49 54.5	-73 30 05	5	-	6	2	38	17	25	17	1x1	0.28	0.62	9.9	17.0	00499-7330	C	
77	00 50 03.0	-73 06 55	5	-	7	2	50	30	-	-	1xp	0.23	0.66	8.8	C	00500-7306	H	
78	00 50 09	-72 57	3	-	4	2	-	-	-	-	-	0.11:	0.22	C	C		H	
79	00 50 09.7	-72 22 14	-	-	-	-	8	4	4	3	-	-	-	1.7	2.1	00501-7222	C	
80	00 50 18.2	-72 20 02	-	-	-	-	6	3	6	3	-	-	-	1.2	6.3	00503-7220	C	
81	00 50 22	-72 35	-	-	-	-	17	9	14	6	4x4	-	-	8.8	28.0		C	
82	00 50 25.9	-73 53 09	-	-	2	-	15	6	10	6	2x2	-	0.50	5.6	9.8	00504-7353	C	
83	00 50 36	-72 57	-	-	4	2	44	15	25	10	5x4	-	1.18	37.0	59.0		C	
84	00 50 38 1	-72 07 39	-	-	-	-	4	2	4	2	10x3	-	-	3.8	11.0	00506-7207	C	
85	00 50 46 4	-72 45 56	-	-	1	-	12	9	10	8	-	-	0.11:	1.2	4.2	00507-7245	C	
86	00 50 54 7	-73 42 47	7	-	10	1	30	15	21	13	p	0.26	1.00	6.2	17.0	00509-7342	C	
87	00 51 15.2	-72 29 46	-	-	-	-	17	9	11	6	3x3	-	-	6.7	15.0	00512-7229	C	
88	00 51 18	-73 39	3	-	6	2	36	17	30	18	2xp	0.19:	0.71	9.7	27.0		C	
89	00 51 23	-73 23	5	-	-	-	-	-	-	-	p:	0.19	-	C	C		S	SAO 255715
90	00 51 24	-74 46	10	-	-	-	-	-	-	-	p	0.37	-	-	-	00515-7455:	S	SAO 25571e

TABLE IV (*continued*).

(1)	(2)		(3)		(4)		(5)		(6)		(7)	(8)	(9)	(10)	(11)	(12)	(13)	(14)
Number	Position RA(1950) h m s	DEC(1950) ° ′ ″	12 μm Peak	Bg	25 μm Peak	Bg	60 μm Peak	Bg	100 μm Peak	Bg	Size arcmin	F 12μm Jy	F 25μm Jy	F 60μm Jy	F 100μm Jy	IRAS-Id	Spec-trum	Comments
					10^{-8} Watt $m^{-2}sr^{-1}$													
91	00 51 24	-73 01	-	-	6	2	-	-	-	-	p	-	0.44	C	C		H	
92	00 51 38.4	-72 59 12	5	-	5	2	36	20	23	20	p:	0.19:	0.33	6.6	6.3	00516-7259	H	
93	00 51 47.9	-72 40 19	-	-	1	-	17	10	10	7	3x5	-	0.51:	7.7	11.0:	00517-7240	C	
94	00 51 56.0	-72 55 35	5	-	6	2	42	20	24	12	2x3	0.57	1.22	16.0	32.0	00519-7255 X0051-729	C	
95	00 52 00	-73 10	-	-	2	-	17	10	-	-	-	-	0.22	2.9	C		H	
96	00 52 04	-72 59	5	-	-	-	-	-	-	-	-	0.19:	-	C	C		S	
97	00 52 06	-73 00	5	-	2	-	-	-	-	-	-	0.19	0.22:	C	C		H:	
98	00 52 12	-73 36	7	-	11	2	30	17	-	-	p	0.26	1.00	5.4	C	00524-7335: X0052-735	M	
99	00 52 17.7	-73 05 43	-	-	2	-	25	16	16	12	p:	-	0.22	3.7	8.4	00522-7305	C	
100	00 52 21	-73 38	3	-	4	-	-	-	-	-	p	0.11:	0.44	C	C		H	
101	00 52 25.2	-71 53 26	13	-	-	-	-	-	<1	-	p	0.48	-	-	-	00524-7153	S	
102	00 52 36.0	-72 45 15	5	-	6	-	22	15	14	10	4x1	0.58	1.86	5.2	11.0	00525-7245	C	
103	00 53 16.3	-72 44 11	-	-	2	-	18	15	-	-	-	-	0.22:	1.2	C	00532-7244	H	
104	00 53 21.4	-74 34 35	18	-	-	-	-	-	-	-	p	0.67	-	-	-	00533-7434	S	SAO 255721
105	00 53 31.0	-72 55 00	-	-	2	-	25	16	16	12	3x4	-	0.87:	8.6	13.0	00535-7255	C	
106	00 53 46	-72 58	5	-	-	-	-	-	-	-	-	0.19	-	C	C		S	
107	00 54 12.7	-73 34 43	31	-	5	-	-	-	-	-	p	1.15	0.56	C	C	00542-7334	S	
108	00 54 16.7	-72 21 00	-	-	-	-	10	7	8	6	4x3	-	-	2.9	6.4	00542-7220	C	
109	00 54 18	-72 37	3	-	2	-	31	20	-	-	p:	0.11:	0.22:	4.5	C		H	
110	00 54 28	-72 34	5	-	2	-	32	13	22	15	4x3	0.82	0.87	18.0	22.0		C	
111	00 54 28.6	-73 03 04	5	-	6	1	32	15	-	-	px1	0.23:	0.66	7.5	C	00544-7303	H	
112	00 54 32	-73 23	-	-	2	-	-	-	-	-	p:	-	0.22	C	C		H	
113	00 54 49	-72 39	-	-	3	1	27	17	21	15	p:	-	0.22	4.1	13.0		C	
114	00 55 00	-72 47	3	-	2	1	22	17	16	13	p:	0.11:	0.11	2.1	6.3		C	
115	00 55 00	-73 03	2	-	2	-	29	15	22	12	2x3	0.23:	0.61	10.0	27.0	X0055-730	C	
116	00 55 03	-72 56	-	-	2	-	-	-	-	-	-	-	0.22	C	C		H	
117	00 55 10	-73 04	3	-	2	-	27	15	23	12	5x1	0.41:	0.74	10.0	34.0		C	
118	00 55 18.6	-73 17 02	-	-	-	-	9	5	8	6	-	-	-	1.7	4.2	00553-7317	C	
119	00 55 24.8	-73 51 29	12	-	2	-	-	-	-	-	p	0.44	0.22	C	C	00554-7351	S	
120	00 55 30	-73 02	3	-	-	-	-	-	-	-	-	0.11:	-	C	C		S	
121	00 55 47.8	-72 48 41	5	-	10	1	34	17	18	15	p	0.19:	1.00	7.0	6.3	00557-7248	M	
122	00 55 57	-73 10	5	-	2	-	-	-	-	-	-	0.19	0.22	C	C		H	
123	00 56 00	-72 16	-	-	-	-	13	10	-	-	-	-	-	1.2:	C		H	
124	00 56 17.1	-72 55 23	5	-	8	1	35	13	21	13	p	0.19	0.78	9.1	17.0	00562-7255	C	
125	00 56 22.7	-72 20 22	3	-	5	2	21	12	16	10	p	0.11:	0.33	3.7	13.0	00563-7220	C	
126	00 56 34	-72 42	-	-	2	-	27	20	24	15	px2	-	0.35:	3.6	20.0		C	
127	00 56 40	-72 27	5	-	15	2	-	-	-	-	-	0.19:	1.44:	C	C		M	
128	00 56 41	-72 56	5	-	6	-	35	13	-	-	p	0.19	0.67	9.1	C		M	
129	00 56 45	-72 52	-	-	2	-	23	16	16	12	p.	-	0.22:	2.9	8.4		C	
130	00 56 59.9	-72 43 43	10	-	20	2	36	18	-	-	p	0.37:	2.00	7.4	C	00569-7243	M	
131	00 57 26.5	-72 26 36	43	-	120	2	260	20	93	10	3x3	5.99	43.50	200.0	242.0	00574-7226 X0057-724	C	
132	00 57 28.4	-73 09 12	-	-	-	-	12	9	-	-	-	-	-	1.2	C	00574-7309	H	
133	00 57 42	-72 31	5	-	6	2	-	-	-	-	-	0.19:	0.44:	C	C		M	
134	00 57 54	-72 03	-	-	1.5	-	13	6	10	5	3x3	-	0.55:	5.8	15.0		C	
135	00 58 06	-72 25	5	-	12	10	70	20	-	-	-	0.19:	0.22	21.0	C		H	
136	00 58 12	-71 47	-	-	1.5	-	7	3	7	5	px2	-	0.27:	2.0	4.5		C	
137	00 58 12	-72 24	-	-	12	4	60	15	-	-	p	-	0.89	19.0	C		M	
138	00 58 36	-72 05	-	-	2	-	17	10	13	9	2x3	-	0.61:	5.0	11.0		C	
139	00 59 06	-73 07	5	-	1	-	6	5	-	-	p:	0.19	0.11:	0.4	C		M	
140	00 59 10	-71 55	5	-	-	-	-	-	-	-	p:	0.19	-	C	C		S	
141	00 59 13.2	-72 58 17	18	-	1.5	-	-	-	-	-	p	0.67	0.17:	-	-	00592-7258	S	SAO 255729
142	00 59 18.4	-71 51 24	5	-	9	1	26	5	14	5	p	0.19	0.89	8.7	19.0	00593-7151	C	
143	00 59 25	-72 04	-	-	2	-	-	-	-	-	-	-	0.22	C	C		H	
144	00 59 27.9	-71 44 06	-	-	-	-	8	4	4	2	p	-	-	1.7	4.2	00594-7144	C	
145	00 59 51.8	-71 49 03	9	-	-	-	-	-	-	-	p	0.33	-	-	-	00598-7149	S	SAO 255730
146	00 59 52.2	-72 06 50	-	-	8	1	26	13	16	10	p	-	0.78	5.4	13.0	00598-7206	C	
147	00 59 56.1	-72 12 16	-	-	1.5	1	20	13	16	15	-	-	0.06	2.9	2.1	00599-7212	M	
148	01 00 04.8	-72 03 07	-	-	-	-	13	10	-	-	p.	-	-	1.2	C	01000-7203	M	
149	01 00 05.5	-71 55 32	-	-	1.5	-	7	4	6	5	p:	-	0.17:	1.2	2.1	01000-7155	C	
150	01 00 27	-74 17	5	-	-	-	-	-	-	-	-	0.19:	-	-	-		S	
151	01 01 00	-73 13	-	-	-	-	6	4	5	3	-	-	-	0.8	4.2		C	
152	01 01 09.3	-72 09 42	10	-	11	2	42	16	29	16	p	0.37	1.00	11.0	27.0	01011-7209	C	
153	01 01 12.8	-72 41 34	-	-	2	-	17	7	11	7	3x2	-	0.61:	7.2	11.0	01012-7241	C	
154	01 01 18	-72 14	5	-	5	2	30	20	-	-	p	0.19	0.33	4.1	C		H	
155	01 01 19	-72 18	11	4	10	3	-	-	-	-	p	0.26	0.78	C	C		H	
156	01 01 31.0	-72 22 16	10	-	8	2	-	-	-	-	p	0.37	0.67	C	C	01015-7222	M	
157	01 01 32.0	-72 56 42	-	-	-	-	7	5	6	5	-	-	-	1.2	2.1:	01015-7256	C	
158	01 01 32.8	-71 06 59	18	-	-	-	-	-	-	-	p	0.67	-	-	-	01015-7106	S	NGC 362
159	01 01 38	-73 30	5	-	-	-	4	2	3	2	-	0.19:	-	0.8	2.1		C	
160	01 01 41.9	-72 28 06	-	-	6	2	25	14	16	15	p	-	0.44	4.5	2.1	01016-7228	M	
161	01 01 42	-72 20	10	-	13	3	75	20	46	15	p:	0.37	1.11	23.0	65.0		C	
162	01 02 11.2	-72 19 19	5	-	17	3	85	20	-	-	p	0.19	1.55	27.0	C	01021-7219	M	
163	01 02 13.4	-72 24 53	-	-	4	1.5	26	17	18	15	p	-	0.28	3.7	6.3	01022-7224	C	
164	01 02 27.8	-73 43 47	5	-	-	-	-	-	-	-	-	0.19	-	-	-	01024-7343	S	
165	01 02 44.9	-72 07 39	3	-	2	-	18	15	16	14	-	0.11:	0.22:	1.2	4.2	01027-7207	C	
166	01 02 51.4	-73 10 15	-	-	1	-	5	3	5	3	-	-	0.11:	1.2	4.2	01028-7310	C	
167	01 03 30.1	-72 00 08	12	-	1.5	-	-	-	-	-	p	0.44	0.17:	C	C	01035-7200	S	SAO 255735
168	01 03 30.3	-72 15 28	37	-	100	2	128	20	43	15	p	1.37	10.90	45.0	59.0	01035-7215	C	
169	01 03 36.3	-72 40 39	-	-	-	-	9	5	7	5	p	-	-	1.7	4.2	01036-7240	C	
170	01 03 44	-72 25	-	-	2	-	20	15	13	12	p	-	0.22	2.1	2.1		M	
171	01 03 48.5	-71 12 03	10	-	-	-	-	-	-	-	p	0.37:	-	-	-	01038-7112	S	SAO 255738
172	01 03 50	-72 12	-	-	4	1.5	20	18	-	-	p	-	0.28	0.8	C		H	
173	01 03 56.9	-73 05 59	5	-	9	-	13	4	6	3	p	0.19	1.00	3.7	6.3	01039-7305	C	
174	01 03 59.2	-72 46 34	-	-	-	-	10	5	7	5	2x2	-	-	3.1	4.9	01039-7246	C	
175	01 04 06	-72 20	3	-	4	2	30	17	20	17	p	0.11:	0.22	5.4	6.3		C	
176	01 04 13.9	-72 15 51	5	-	12	2	35	15	-	-	p	0.19	1.11	8.3	C	01042-7215	H	
177	01 05 06	-73 24	-	-	-	-	5	2	4	3	-	-	-	1.2	2.1		C	
178	01 05 24	-72 51	-	-	-	-	11	5	9	5	2x2	-	-	3.7	9.8		C	
179	01 05 26.4	-73 07 22	5	-	2	-	7	3	6	3	p:	0.19:	0.22:	1.7	6.3	01054-7307	C	
180	01 05 45	-74 04	7	-	-	-	-	-	-	-	p	0.26:	-	-	-		S	

TABLE IV (*continued*).

(1)	(2)		(3)		(4)		(5)		(6)		(7)	(8)	(9)	(10)	(11)	(12)	(13)	(14)
Number	Position RA(1950) h m s	DEC(1950) ° ′ ″	12 μm Peak	Bg	25 μm Peak	Bg	60 μm Peak	Bg	100 μm Peak	Bg	Size arcmin	F 12μm Jy	F 25μm Jy	F 60μm Jy	F 100μm Jy	IRAS-Id	Spec-trum	Comments
					10^{-8} Watt $m^{-2}sr^{-1}$													
181	01 06 01.5	-72 50 21	-	-	1.5	-	11	5	8	7	p:	-	0.17:	2.5	2.1:	01060-7250	M	
182	01 06 41	-73 10	5	-	-	-	-	-	-	-	p.	0.19	-	C	C		S	NGC 419
183	01 06 46.1	-72 28 09	-	-	-	-	9	4	5	4	p.	-	-	0.8	2.1	01067-7228	C	
184	01 06 58.3	-72 15 46	-	-	5	1	26	6	18	6	3x3	-	1.48	17.0	35.0	01069-7215	C	
185	01 07 27.8	-71 40 06	11	-	4	-	-	-	-	-	p	0.41	0.44	-	-	01074-7140	M	
186	01 07 33.8	-72 54 39	70	-	7	-	4	3	-	-	p	2.59	0.78	0.4	C	01075-7254	S	
187	01 07 43.9	-73 27 40	12	-	23	-	46	2	16	3	p	0.44	2.55	18.0	27.0	01077-7327	C	
188	01 07 45.2	-72 45 35	-	-	-	-	5	3	-	-	-	-	-	0.8	-	01077-7245	M	
189	01 08 03.6	-72 37 25	-	-	-	-	6	3	4	3	2x2:	-	-	1.9	2.5	01080-7237	C	
190	01 09 18	-72 58	-	-	-	-	6	3	5	3	4x4	-	-	3.3	7.1		C	
191	01 09 27.6	-71 52 26	27	-	1.5	-	-	-	-	-	p	1.00	0.17:	-	-	01094-7152	S	
192	01 09 30	-73 21	-	-	-	-	4	2	5	3	-	-	-	0.8	4.2		C	
193	01 09 31.4	-72 25 33	-	-	3	-	7	3	5	3	p	-	0.33	1.7	4.2	01095-7225 X0110-724 *	C	
194	01 09 50.3	-72 38 47	-	-	6	-	13	3	7	3	1x1	-	0.93	4.7	8.7	01098-7238	C	
195	01 10 41.3	-73 00 12	-	-	-	-	8	3	6	3	2x2	-	-	3.1	7.4	01106-7300	C	
196	01 10 44	-74 11	5	-	-	-	-	-	-	-	p:	0.19:	-	-	-		S	SAO 255751
197	01 11 39.0	-72 26 36	-	-	-	-	4	2	2	1	p:	-	-	0.8	2.1	01116-7226 X0110-724 *	C	
198	01 12 10.9	-71 08 07	8	-	-	-	-	-	-	-	p	0.30	-	-	-	01121-7108	S	
199	01 12 29.2	-73 32 49	17	3	22	2	117	6	60	4	p	0.52	2.22	46.0	117.0	01124-7332 X0112-735 *	C	
200	01 12 41.2	-73 32 42	22	3	38	2	-	-	-	-	p:	0.70	4.00	C	C	01126-7332 X0112-735 *	M	
201	01 13 19.1	-73 33 42	10	2	20	2	-	-	-	-	p	0.30	2.00	C	C	01133-7333 X0112-735 *	M	
202	01 13 23.1	-73 36 33	11	2	22	2	83	6	48	6	p	0.33	2.22	32.0	88.0	01133-7336	C	
203	01 13 56.5	-72 34 44	-	-	-	-	2	1	2	1	-	-	-	0.4	2.1	01139-7234	C	
204	01 14 17.3	-73 27 38	5	-	4	1	21	6	14	9	p:	0.19:	0.33	6.2	10.0	01142-7327	C	
205	01 14 18.1	-73 26 04	-	-	4	-	-	-	-	-	p	-	0.44	C	C	01143-7326	M	
206	01 15 00	-73 45	-	-	-	-	4	2	3	2	-		-	0.8	2.1	X0115-737	C	
207	01 15 21.1	-73 24 14	-	-	-	-	8	6	-	-	p	-	-	0.8	C	01153-7324	M	
208	01 16 06	-73 59	7	-	1	-	-	-	-	-	p	0.26	0.11:	C	C		S	
209	01 16 28.7	-73 11 09	-	-	-	-	3	2	3	2	-	-	-	0.4	2.1	01164-7311	C	
210	01 19 36.8	-73 37 13	-	-	-	-	2	1	2	1	-	-	-	0.4	2.1	01196-7337	C	
211	01 20 00	-74 15	-	-	-	-	1	-	1	-	-	-	-	0.4:	2.1		C	
212	01 20 12	-73 20	-	-	-	-	2	1	2	1	-	-	-	0.4	2.1		C	
213	01 21 37.9	-74 50 50	-	-	-		1	-	<1	-	-	-	-	0.4:	-	01216-7450	M	
214	01 22 24.0	-73 38 54	-	-	-	-	5	2	4	2	1x2	-	-	1.6	4.6	01224-7338	C	
215	01 22 52.8	-73 24 45	42	2	150	2	120	2	24	7	1x1	2.21	22.90	55.0	46.0	01228-7324	M	
216	01 22 56.2	-73 29 43	2	-	1	-	7	4	6	5	-	0.07	0.11	1.2	2.1	01229-7329	C	
217	01 23 24.3	-73 53 31	-	-	2	-	2	-	1	-	p	-	0.22:	0.8	2.1	01234-7353	C	
218	01 24 10.3	-73 40 01	-	-	-	-	8	2	6	3	p.	-	-	2.5	6.3	01241-7340 X0123-736	C	
219	01 24 12.7	-73 30 50	2	-	3	-	9	2	5	3	p	0.07	0.33	2.9	4.2	01242-7330	C	

TABLE V. — *SAO (1966) stars in the field of the SMC.*

(1)	(2)	(3)	(4)	(5)	(6)	(7)	(8)	(9)	(10)
SAO number	m V mag	Sp type	F[a] 12μm Jy	F[a] 25μm Jy	F /F 25μm 12μm	m - m V 12 mag	Infrared Id	Detection[b] quality	Remarks[c]
255682	9.2	K5	-	-	-	-		-	
255683	9.6	F5	0.03:	-	-	2.2		-	
255684	8.6	K5	0.59	0.16	0.27±0.07	4.4	3	+	Faint emission at 60 μm.
255686	8.6	K5	0.31	0.04	0.13±0.1	3.7	4	+	
255689	7.4	F2	0.08	-	-	1.0	7	0	
255690	6.9	A0	0.08	-	-	0.5	8	0	
255692	8.9	A3	0.03:	-	-	1.5		-	
255693	8.9	K5	0.09	0.04	0.44±0.4	2.7		+	
255694	8.5	F0	0.04:	-	-	1.4		-	
255695	9.4	G5	0.01:	-	-	0.8		-	In extended emission.
255698	7.7	F5	0.04:	-	-	0.6		-	
255699	8.5	F0	-	-	-	-		-	
255700	8.3	F5	-	-	-	-		-	
255707	9.5	F5	-	-	-	-		-	In extended emission.
255711	8.8	K0	0.31	-	-	3.9	56	+	In extended emission.
255713	7.1	F2	0.08	-	-	0.7	69	0	
255715	9.0	K0	0.13	-	-	3.2	89	+	In extended emission.
255716	7.8	G0	0.26	-	-	2.7	90	+	
255717	8.5	F8	-	-	-	-		-	
255721	6.8	G5	0.47	0.08	0.17±0.09	2.4	104	+	
255723	8.4	A5	0.04	-	-	1.3		0	
255725	9.1	F5	0.04	0.04	1.00±1.0	2.0		0	
255729	8.0	K0	0.47	0.12	0.26±0.08	3.6	141	+	Close to extended emission.
255730	7.6	K0	0.23	0.08	0.35±0.18	2.4	145	+	Close to extended emission.
255733	8.6	K0	0.08	-	-	2.0		0	In extended emission.
255735	7.5	K0	0.31	0.12	0.39±0.1	2.6	167	+	
255736	8.2	G0	0.08	0.04	0.50±0.5	1.8		0	
255738	7.9	K0	0.26	0.08:	0.31±0.1	2.8	171	+	
255743	8.6	F0	-	-	-	-		-	
255745	9.1	G5	0.10	-	-	3.0		+	
255746	8.0	G0	0.09	-	-	1.8		0	Close to extended emission.
255748	7.2	A0	0.04	-	-	0.1		0	
255751	7.5	F8	0.13	-	-	1.7	196	+	
255752	8.2	G5	0.21	0.04	0.19±0.2	2.9		+	2'W of 198.
255755	9.1	K2	-	-	-	-		-	2'E of N84.
255758	9.4	A0	-	-	-	-		-	
255759	8.6	K0	0.08	-	-	2.2		0	
255761	8.2	F5	-	-	-	-		-	
255763	10.0	G0	0.04	-	-	2.9		0	
255765	7.7	F0	0.04	-	-	0.6		0	
255766	9.0	G0							Not covered by IRAS DPM-map.
255767	8.4	K0	0.12	-	-	2.5		+	
255768	8.1	K0	0.08	-	-	1.7		0	
255769	8.8	F8	-	-	-	-		-	
255773	7.9	A2	-	-	-	-		-	
255774	8.2	A5							Not covered by IRAS DPM-map.
255778	8.6	F2	-	-	-	-		-	

Notes to Table 5:
a) The 12 and 25 μm flux densities in this table are colour-corrected (not in any of the other tables) by dividing the nominal flux densities by 1.43 and 1.40 (correction for a 5000 K black body; for stars with other temperatures these factors are about the same, see IRAS, 1985a).
b) Detection qualities at 12 μm are good (+), medium (0) or poor (-).
c) See Section 5.1.1 in the text.

1989A&AS...79...79S

TABLE VI. — *Radcliffe stars (Feast et al., 1960) in the SMC.*

(1) Radcliffe Id	(2) m[a] V mag	(3) Sp type	(4) F 12μm Jy	(5) Infrared Id[b]	(6) Detection quality	(7) Remarks[c]
1	12.0 V	F8Ia	0 2 :	13:	0	2'S of 13/ 2'W of 16.
2		BoIe	0.1 :	19:	0	On edge of SW-Bar, 2'E of 19/ 3'S of 20.
3		A3:I:(e)	< 0.08:		-	
4		Be	-		-	In SW-Bar, on border of N19. 3'SE of 36.
5	11.0	B3I	0 2 :		-	In SW-Bar.
6	10.96	B6I	< 0.2 :		-	On edge of SW-Bar.
7	12.0 V	G0:I	< 0.2 :		-	2'N of 66/ 3'W of 74.
8	11.11	A0Ia:	0.2		-	On edge of SW-Bar.
9	10.98	B3Ia:	-		-	On edge of SW-Bar, 1'NE of R8.
10	10.91	A0Ia:	0.2	89:	-	0.3'SW of SAO 255715 (see Table 5).
11	10.75	B6Ia	-		-	In extended emission, on edge of N50.
12	12.2 V	F8Ia	-		-	
13		A3:Ia:(e)	< 0.08:		-	
14	11.61	Hp	0.2 :	135:	-	In N66, 2'NE of 131/1'W of 135/2'SW of 137.
15		(A-B)e	< 0.08:		-	
16		B	< 0.04:		-	
17	12.12	B0I	-		-	
18		B0.5I	-		-	Near edge of N66, 5'SE of 131.
19		A3Ia	-		-	3'NW of 142.
20	12.3 V	K5Ia:e	-		-	
21		A0Ia:	-		-	
22	12.27	A3I	-		-	
23		A1I	-		-	
24	12.50	A0:	0.2 :		-	Close to N76.
25		B1:	-		-	2'E of R23.
26		F0Ia:	0.2 :		-	Edge of N76.
27	10.9	B9Ia	< 0.08:		-	3'W of 160.
28		B0I	0.4	161	-	Border of N76, 1'W of R30.
29	12.74	K.	0.4	156	-	In N76, 1'W of R31.
30	13.2	Be	0.2 :	161	-	In N76, 1'E of R28.
31	12.3	O:f:	0.4	156	-	In N76, 1'E of R29.
32		B	0.2	162	-	In N76, 2'SW of R35.
33		B	< 0.08:	163	-	Edge of N76, 1'N of 163.
34	12.83	F0 I(e)	-		-	Non-SMC member (Azzopardi and Vigneau, 1982).
35		B1I:	0.2 :	162	-	Border of N76, 2'NE of R32.
36	11.26	B3I	< 0.08:		-	
37	11.20	B0I	< 0.08:		-	
38		Pec	-		-	
39		B2:I(e)	-		-	
40	10.73	B8Ie	< 0.08:		-	
41		Be	-		-	3'SW of 187.
42	10.95	B2.5I	-		-	
43		A2I	-		-	
44[d]		Neb	0.4	187	-	Position of HDE 7113 (N81), 0.4'SE of 187.
45	10.13	A0Ia-0	-		-	4'SW of 209/210.
46	V	G0	-		-	
47	11.56	FIe				Not covered by IRAS OPM-map.
48		e				Not covered by IRAS OPM-map.
49		(A-B)e				Not covered by IRAS OPM-map.
50	11.56	Pec				Not covered by IRAS OPM-map.

Notes to Table 6:
a) Magnitudes followed by a V indicate that the star is variable, the average of the maximum and minimum magnitudes are given in those cases.
b) Only associations 13, 19 and 89 from Table 4 have S-type infrared spectra, all others are associated to entries in Table 7 (HII regions). Infrared sources 156, 161, 162 and 187 have emission at other IRAS wavelength bands than 12 μm.
c) See Section 5.1.2 in the text.
d) According to Feast et al. (1960) R44 corresponds to N81/HDE 7113. We find that their Table 2 coordinates are 9'N of N81. Here we used the N81 (HII region) coordinates (Henize, 1956).

TABLE VII. — *Infrared emission from H-alpha Emission Nebulae in the SMC (Davies et al., 1976; Henize, 1956).*

(1) DEM Id	(2) Henize Id	(3) Intensity of H-alpha	(4) Infrared Id[a]	(5) Detection quality	(6) Remarks[b]
1	N 3	b			Not covered by IRAS OPM-map.
2		f	6	+	
3		b		0	On edge of IR extended emission.
4		b		0	On edge of weak IR extended emission.
5		vf	10	+	Offset 2'N. (Def: Offset=Pos(H-alpha)-Pos(IR)).
6		f+b	15	+	Offset 1'N.
7		b	16	+	
8		b		-	On edge of IR extended emission.
9	N 9	b	23	+	
10		f		+	Filament along edge of IR extended emission.
11	N10	b	26	+	Offset 1'N.
12		vf	24	0	Center H-alpha shell 3'NE.
13		f+b	26	+	IR 26 on N extension of H-alpha nebula; No IR peak on main body.
14		b	27	+	Offset 2'N.
15	N12 (part)	b	30	+	Offset 1'NW.
16	N13A,B	vb	29	+	
17		f+b	28	+	
18	N12B	b	30	0	Offset 2'N.
19		vf	31	+	IR coincides with southern part of nebula.
20	N12 (part)	b		0	On edge of IR 36.
21	N16	f+b	35	+	IR source on bright part of shell.
22		fb		+	Shell lining edge of IR 'hole'.
23	N12A	vb	36	+	
24		b		-	2'N of IR 35.
25	N17	b	38	+	
26		b		-	
27		fb		-	Near edge of IR 38.
28	N15	b		-	On edge of IR 29.
29		f	44,37	0	Delineating edge of extended IR emission, IR 44 coincides with E peak.
30		b		-	
31	N19	b		-	On edge of IR 49.
32		vb	43	0	IR follows nebular outline.
33		f	46	+	Nebulae on edge of IR emission.
34		fb		+	IR confused area: DEM 34, 35 and 36.
35		fb	42	+	IR peak 42 in between.
36		b		+	IR confused area: DEM 34, 35 and 36.
37	N22	b	45	+	IR peak 45 in between 37 and 38.
38	N25,N26	vb		+	IR peak 45 in between 37 and 38.
39		b		0	Coincides with IR 'hole'.
40	N27	b	49	+	
41		b		-	
42	N24	vb		-	On IR gradient (to IR 45 and 42).
43		b		-	On IR gradient (to IR 45).
44		f	52,56,57	+	IR peaks on East part of H-alpha nebulae.
45	N30	vb	51	+	Offset 3'NE.
46		f	48	+	IR on NW part of nebula.
47		f		-	On IR gradient (to IR 63).
48	N32	b	58	+	
49		f+b	54	+	Shell borders on IR extended emission.
50		b		-	On edge of extended emission.
51		vf	59	+	On extended emission.
52		b	68	+	Offset 2'W.
53		f	70	+	IR source in S of H-alpha nebula only.
54	N36,N41	vb	65	+	Shell coincides with extended IR source.
55	N37	vb	66	+	
56		b	62	+	
57	N35	b		0	On N edge of 62.
58		vf		-	On edge IR extended emission, in IR-hole.
59		fb	73	+	
60	N45	b	76	+	
61		b		0	On edge of IR extended emission.
62	N46	b	77	+	
63		fb	78	0	Edge of extended emission.
64		vf		0	Bright SE component coincides with IR peak.
65		fb		+	Extended IR emission peak of IR 81.
66		fb	75,79,80,87	+	IR complex at edge of extended emission.
67		fb	84	+	Center shell offset 2'W.
68	N50	b		0	On edge of IR 92,94 complex/pair.
69		fb		+	Weak IR emission.
70		fb		0	Edge of IR emission.

TABLE VII (*continued*).

(1) DEM Id	(2) Henize Id	(3) Intensity of H-alpha	(4) Infrared Id	(5) Detection quality	(6) Remarks
71	N48	b		0	On edge of IR 86.
72	N51	b	86	+	
73		fb		0	3'NE of IR 86.
74		vf	88,98	+	SE peak coincides with IR peak 98, N with 88.
75		vb		-	
76		fb	93	-	Offset 2'E.
77	N52A,B	b	94	+	
78		b		+	Weak IR emission.
79		vf		0	Edge of IR emission.
80		fb	105,106	+	Main source coincides with IR 'hole', bright part with IR 105.
81		f		-	Edge of IR extended emission.
82		b		0	On edge of IR 111.
83	N57	b		0	On edge of IR 110.
84		fb		0	On edge of IR 110.
85	N58	b	110	+	
86		fb	109	+	
87		f	114	0	
88		f	111	+	
89		vf	117	+	Follows extended IR emission, close to IR 111.
90		f		+	Shell follows edge of IR extended emission.
91	N59	b	119	+	Offset 1'N.
92		b		-	
93	N62	vb		+	Offset 3'SW of IR 124.
94	N63	vb	124	+	
95	N64A	vb	128	0	IR 128 in between DEM 94,95.
96		f		0	Edge of extended IR emission.
97		f		-	
98		fb		+	On IR gradient (to IR 131).
99		fb	133	+	On IR gradient (to IR 131).
100	N69	b		0	Extended IR emission.
101		f		-	
102		b		-	Edge of IR 131.
103	N66A,B,C,D	vb	131,135,137	+	IR 131 source covers only SW part of very large nebula. IR 135 and 137 are in centre of NE part.
104		vf		-	In extended emission.
105		f		-	On edge IR extended emission.
106	N69	b		+	Weak IR emission.
107		b	128	+	
108		f	130	+	Weak extended IR source.
109	N71	vb	142	+	
110		b	144	+	
111		fb	147	+	Offset 3'SW.
112	N72	b	146	+	Offset 2'SW.
113		fb	148	+	Offset 2'SW.
114		f		+	Nebular filament delineates edge of IR 'bay'.
115	N74	b		-	On edge of IR 152.
116	N75	b		-	
117a,b	N77B,A	b,vb	152	+	DEM 117b coincides with IR 152.
118		b	153	+	IR 153 lies on arc DEM 118.
119		b	156	+	1'W of IR 156.
120	N76B	vb	156	+	1'S of IR 156.
121		b		-	Edge of IR 152.
122		f		-	On edge IR extended emission.
123	N76A	vb	160,161, 162,163	+	Complex.
124		fb		0	Shell around H-alpha corresponds with IR emission.
125		f	169	+	Confused. H-alpha follows IR emission.
126	N78A,B	vb	168	+	Offset 2'S.
127	N78D	vb	168	+	Offset 1'E.
128		f	170	+	
129		fb	173	+	Offset 1'N.
130	N78C	vb		+	Weak IR peak.
131		b		0	Edge of weak IR peak.
132		fb		-	IR extended emission.
133		f	179	+	
134		fb	174,178,181	+	Complex.
135	N80	b	184	+	IR 184 lies on brighter E part.
136		f		-	Edge of extended IR emission.
137		fb	189	+	Offset 1'N.
138	N81	f+b	187	+	Offset 3'N.
139		vf	188	+	IR peak N of S-part; IR extended emission follows main source.
140		fb	190	+	Weak extended IR peak.
141		b	194	+	
142		b	193	+	3'SE of IR 193.
143		vf		0	Weak IR extended level.
144		fb	195	+	Shell at offset 2'N.
145		vf		+	Weak IR extended emission.
146		f+b		+	Weak IR peak.
147	N83A,C	vb		+	On extension of IR 199.
148	N83B	vb	199	+	
149	N84C	vb	200	+	
150	N84 (part)	b		0	Edge of IR 199, 200.
151	N84A	vb	201	+	Confused.
152	N84B,D	vb	202	+	Confused.
153		f		0	Weak extended IR emission.
154		fb	203	+	Offset 3'S.
155		b	204,205	+	
156		b		0	On extension of IR 204/205.
157		f		0	Filaments (follow it partially). IR 206 on S filament.
158		fb	207	+	Offset 1'S.
159		b		-	Edge of IR complex.
160		fb	214	+	IR between H-alpha peaks.
161	N88	vb	215	+	
162		f		0	Weak IR emission.
163		f	216,219	0	Confused.
164	N89	b	218	+	Shell around IR peak.
165		vf		-	On edge IR extended emission.
166	N90	vb			Not covered by IRAS DPM-map.
167		f			Not covered by IRAS DPM-map.

Notes to Table 7.
a) Associations 48, 54, 56, 106, 119 from Table 4 have S-type infrared spectra. All other associated infrared sources have C-type or M-type infrared spectra.
b) See Section 5.2 in the text.

TABLE VIII. — *Clusters in the SMC (Kron, 1956; Lindsay, 1958; Hodge and Wright, 1972), with infrared counterparts.*

(1) Name[a]	(2) Other names	(3) F 12μm Jy	(4) F 25μm Jy	(5) F 60μm Jy	(6) F 100μm Jy	(7) Infrared Id[b]	(8) Detection quality	(9) Remarks[c]
K 12	L16, NGC176	0.07:	-	-	-		-	At edge, 3.7'SE of 1.
K 14	L18	-	0.4 :	2.5	3.0	6	-	0.6'SW of 6.
K 25	L35	0.1 :	-	-	-		-	At edge of SW Bar.
K 26	L37, NGC269	0.04:	0.2 :	-	-		-	At edge of SW Bar.
K 28	L43	0.06:	-	2.4:	12:		-	
K 31	L46	0.1 :	-	-	-		-	At edge of Bar.
K 33	L50, NGC306	0.06:	-	-	-		-	At edge of Bar.
K 35	L54, NGC330	0.15	0.04:	-	-		+	In Bar.
K 39	L60, NGC346	6	44	200	242	131	-	N66, 0.7'S of 131.
K 48	L71, NGC371	0.4	1.1	23	65	161	-	N76, 0.6'S of 161.
K 51	L75, NGC395	1.4	11	45	59	168	-	N78, 0.2'S of 168.
K 54	L79	0.07:	-	-	-		-	
K 57	L86	0.1 :	0.07	-	-		0	
K 58	L85, NGC419	0.2	0.1	C	C	182	+	1.4'N of 182.
K 64	L89, IC1660	0.04:	-	-	-		-	
K 65	L94, NGC456	0.5	2.2	46	117	199,200	-	0.7'NE of 199, 0.7'NW of 200.
K 66	L97, NGC460	0.3	2.0	C	C	201	-	0.6'SE of 201.
K 67	L99, NGC465	0.1 :	0.2 :	6:	31:		-	
L 41		0.2	0.2 :	C	C	74	0	1.4'N of 74; In Bar.
L 84		0.06:	1.5	17	35	184	-	0.8'NW of 184.
L101		2.2	23	55	46	215	-	1.1'E of 215.
L103		0.07:	0.33:	2.9	4.2	219	-	1.5'NW of 219.
L104		0.04:	0.22:	2.5	6.3	218	-	2.0'NE of 218.
HM16		<0.07	0.1 :	1.2	2.1	16	-	0.8'SW of 16.
HM25		0.06:	-	-	-		-	
HM36		-	-	0.1	0.6		0	
HM37		0.06:	0.6 :	6	15	134	-	1.7'NW of 134.
HM38		-	-	0.1:	0.6		0	
HM41		0.07:	-	-	-		0	
HM46		0.05:	-	-	-		0	
HM60		-	-	1.9	2.5	189	-	0.3'NW of 189.
HM72		<0.06	0.4	C	C	205	-	0.8'N of 205.
HM74		<0.06	0.2:	0.8	C	207	-	0.4'SE of 207.
HM75		0.1 :	-	-	-		0	
HM78		<0.06	-	0.4	2.1	212	-	0.5'SW of 212.
HM81		2.2	23	55	46	215	-	0.4'N of 215.
HM82		2:	20:	50:	40:	215:	-	1.9'SE of 215.

Notes to Table 8:
a) Only clusters which have possible infrared counterparts are given.
b) Only infrared associations 74, 134, 182 and 212 (in Table 4) were not previously included in Table 7 (HII regions). The other infrared associations have clusters and HII regions in a single beam, and thus are confused.
c) See Section 5.3 in the text.

TABLE IX. — *Know supernova remnants in the SMC (Mathewson et al., 1983).*

(1) SNR Cat. number	(2) Infrared Id[a]	(3) SNR size arcsec	(4) Detection quality	(5) Remarks[b]
0045-73.4	3.2'W of 43 3.8'SE of 36	100x 70	-	In SW Bar, in extended emission between 36 and 43.
0046-73.5	3.1'SE of 42 4.6'N of 44 4.3'S of 45	120x 84	-	In SW Bar, close to edge of 42.
0049-73.6	2.9'SE of 68 3.0'NE of 70	110x 80	-	In SW Bar, in infrared hole.
0101-72.4	2.3'N of 160 2.7'W of 163 3.6'S of 156	98x 77	0	6'S of N76, on infrared extension. Probably 160.
0102-72.3	1.7'NE of 162 3.8'NE of 161	24x 24	-	In between N76 and N78.
0103-72.6	1.5'N of 169	292x187	0	On peak of 169.

Notes to Table 9:
a) All associations with Table 4 within 5' are given and all of them have C-type or M-type infrared spectra. All these associations have already been listed in Table 7 (HII regions).
b) See Section 5.4 in the text.

TABLE X. — *Planetary nebulae in the SMC (Sanduleak et al., 1978 ; Sanduleak and Pesch, 1981).*

(1) Number	(2) F 12μm Jy	(3) F 25μm Jy	(4) F 60μm Jy	(5) F 100μm Jy	(6) Infrared Id[a]	(7) Detection quality	(8) Remarks[b,c]
1							Not covered by IRAS DPM-map.
2							Not covered by IRAS DPM-map.
3	-	-	0.2:	1		0	At end of extension of 1 (in Table 4).
4							Not covered by IRAS DPM-map.
5	-	0.1	0.1	C		+	In weak extended emission at edge of SM Bar.
6	0.06:	0.2:	0.4:	C	12	+	N 6, Ln 33, 0.5'N of 12. In weak extended emission of SM Bar.
7	-	-	-	-		-	At edge of SM Bar.
8	-	-	-	-		-	At edge of extended emission.
9	0.6	1.9	28	54	29	0	Ln 66, 1.1'S of 29. Peak in SM Bar.
10						-	At edge of SM Bar.
11	0.2	1.0	4.5	4.2	50	+	N29, Ln115, 0.3'N of 50. In SM Bar.
12	-	-	-	-		-	
13	-	-	-	-		-	At edge of SM Bar.
14	-	-	-	-		-	On edge of SM Bar.
15	<0.05	0.1	-	-		0	
16	-	-	-	-		-	In infrared-hole at 60 and 100 μm.
17	-	0.1	0.25	0.8		+	Weak infrared emission, far North from SMC Bar.
18	-	-	-	-		-	In SM Bar.
19	<0.05	0.44	C	C	91	+	Ln239, 0.2'SE of 91. In SM Bar.
20							Not covered by IRAS DPM-map.
21	-	-	-	-		-	In SM Bar.
22	-	-	-	-		-	Edge of Bar.
23	-	-	-	-		-	Ln343, at edge of SM Bar.
24	-	-	-	-		-	10'N of N66, in extended emission around N66.
25	-	-	-	-		-	Edge of Bar, 7'SW of 142.
26	<0.06	-	<0.1	-		0	In weak extended emission.
27	<0.06	0.1	0.4	1		+	In weak extended emission of N88.
28	<0.08	-	-	-		0	Near weak extended emission.
29							Ln 3. Not covered by IRAS DPM-map.
30	0.04:	-	-	-		0	At edge of Bar.
31	-	-	-	-		-	On infrared emission at edge of Bar.
32	-	-	-	-		-	At edge of SM Bar.
33	<0.05	-	-	-		-	0.7'E of 138 (H-alpha association).
34	-	-	-	-		-	

Notes to Table 10.
a) Association 29 (Table 4) with a C-type infrared spectrum was already associated to an HII region (see Table 7), the other three infrared associations have M-type infrared spectra. Except for nebulae 9 and 19 the nebulae are not disturbed by other prominent visible objects in the beam.
b) References to nebulosities (N, see Henize, 1956) and emission-line objects (Ln, see Lindsay, 1961) are made.
c) See Section 5.5 in the text.

TABLE XI. — *Hodge (1974) dark clouds in the SMC.*

(1) Number[a]	(2) Infrared Id[b]	(3) Detection quality	(4) Remarks[c]
1	30	+	1.8'S of 30; On infrared extension in SM Bar.
2	31	+	0.6' NW of 31; In SM Bar.
3	29	+	0.6'E of 29, 0.7'N of 32; In SM Bar.
4	35	+	1.1'W of 35; In SM Bar.
5		+	Infrared emission in SM Bar extended emission.
6		0	1.9'N of 35; On infrared gradient in SM Bar.
7	35	+	0.9'N of 35; In SM Bar.
8		0	On infrared gradient in SM Bar.
9	38	+	0.5'NE of 38; On infrared peak in SM Bar.
10	36	+	1.3'E of 36, Infrared extension towards peak 43; In SM Bar.
11	42	+	1.5'NW of 42; In SM Bar.
12	45	+	0.9'NW of 45; In SM Bar.
13	45	+	1.5'N of 45; In SM Bar.
14		+	1.7'E of 42; On infrared gradient to 42 and 45 in SM Bar.
15	44	0	1.0'E of 44. Weak infrared emission, on edge of SM Bar.
16		0	Weak infrared emission in Bar.
17		0	On infrared gradient to 51; In SM Bar.
18		+	1.1'SE of 58. Infrared extension near 63; In Bar.
19	63	+	1.3'NW of 63; In Bar.
20		+	Weak infrared extension on edge of SM Bar.
21		0	On infrared gradient SE of 62; In Bar. Pos:00h49m09s,-72°50'54".
22		0	On infrared gradient to 63 and 65 in Bar. 1.8'N of 65.
23		0	On infrared gradient to 63 and 65 in Bar. 2.7'NE of 65.
24	74 2	0	2.2'NW of 74; In extended emission of Bar.
25		0	On infrared extended emission around 63.
26	78 2	0	2.2'S of 78; On infrared gradient in Bar.
27		0	1.9'N of 78; On infrared gradient in Bar.
28	81	+	0.8'N of 81; At the edge of the Bar.
29		0	Near edge of infrared extended emission of SM Bar.
30	88	0	1.3'NE of 88. On edge of infrared extended emission of Bar. Pos:00h51m32s,-73°28'06".
31	4	-	Infrared minimum, in extended emission of Bar.
32		0	On edge of infrared extended emission; In SM Bar.
33		0	On edge of infrared extended emission; In SM Bar.
34	4	0	Near edge of 111, in extended emission of Bar.
35	108	+	1.1'S of 108; At the edge of the Bar.
36		0	On edge of extended emission of Bar.
37	130	+	1.0'SW of 130; In Bar. Pos:00h56m51s,-72°44'24".
38	2	-	7'S of N66, 3.6'SW of 133; In extended emission of Bar.
39	2	-	Infrared minimum in extended emission of Bar.
40	1	-	Infrared minimum in extended emission of Bar. Pos:00h58m57s,-72°16'12".
41		0	On extension to 153, edge of Bar. Pos:01h00m05s,-72°40'00"
42		0	Extension of extended emission in Ming.
43		-	On edge along 153, falls in infrared minimum at edge of Bar.
44		0	7'S of N76, extended emission; In between 156, 160, 163 in NW Bar.
45	200	+	Strong infrared emission peak of N83 of Ming; 1.0'E of 200, 1.8'E of 199, 1.9'NW of 201. Pos:01h12m55s,-73°32'56".

Notes to Table 11:
a) In the SM Bar region at 60 and 100 μm the infrared contours follow Hodge's dark clouds numbers 1, 2, 3, 4, 5, 6, 7, 8, 10, 11, 12, 13, 14, 17. An infrared extension is visible East of the SM Bar corresponding to clouds 29, 30, 32, 33.
All associations (with Table 4) in the SM Bar are suspect due to confusion.
Cloud numbers 21, 37, and 40 have somewhat bad positions, numbers 30, 41 and 45 have completely wrong positions in Hodge's Table 1 compared to Plate I (corrected 1950.0 equatorial coordinates are given).
b) All associations have M-type or C-type infrared spectra. Infrared sources 63, 74, 81, 108, 130 were previously included in Table 7 (HII regions).
c) See Section 5.6 in the text.

TABLE A.1 — *Description of the SMC Co-added map characteristics.*

Characteristic (Unit)	Wavelength band 12 μm	25 μm	60 μm	100 μm
Median noise (MJy/sr) [a]	0.04	0.04	0.03	0.05
(10^{-8} Watt m^{-2} sr^{-1})	0.6	0.2	0.09	0.05
Zero-level uncertainty (MJy/sr)	0.04	0.14	0.23	0.7
(10^{-8} Watt m^{-2} sr^{-1})	0.5	0.7	0.6	0.7
Stripe residuals (MJy/sr) [b]	0.04	0.06	0.07	0.2
(10^{-8} Watt m^{-2} sr^{-1})	0.5	0.3	0.2	0.2
Sensitivity (MJy/sr) [c]	0.3	0.3	0.4	0.6
(10^{-8} Watt m^{-2} sr^{-1})	4	2	1	0.5

Notes to Table A.1:

a) *The value of the median noise is influenced somewhat by the extended emission of the SMC itself, but not so much as in Table 3.*

b) *Higher stripe levels than the average level given in the table can occur.*

c) *The sensitivity indicates the intensity limits of Table A.2.*

TABLE A.2. — *Additions to the SMC Infrared Source List.*

(1) Number	(2) Position RA(1950) h m s	DEC(1950) ° ′ ″	(3) 12 μm Peak Bg	(4) 25 μm Peak Bg	(5) 60 μm Peak Bg	(6) 100 μm Peak Bg	(7) Size arcmin	(8) F 12μm Jy	(9) F 25μm Jy	(10) F 60μm Jy	(11) F 100μm Jy	(12) IRAS-Id	(13) Spec-trum	(14) Comments
					10^{-8} Watt $m^{-2}sr^{-1}$									
220	00 14 58	-74 14	5 -	2 -	- -	- -	-	0.19:	0.22:	-	-		S:	SAO 255653
221	00 15 35.0	-73 56 10	5 -	- -	- -	- -	p	0.19	-	-	-	00155-7356	S	
222	00 16 02.3	-73 25 51	- -	2 -	3 -	0.5 -	p:	-	0.22	1.2	1.0	00160-7325	H	
223	00 16 21	-73 28	6 -	- -	- -	- -	p	0.22	-	-	-		S	
224	00 16 21	-74 03	- -	3 -	- -	- -	p:	-	0.33	-	-		H	
225	00 16 35.2	-74 18 54	14 -	3 -	- -	- -	p	0.52	0.33	-	-	00165-7418	S	
226	00 18 05.8	-73 37 30	- -	- -	1.5 -	- -	p:	-	-	0.6	-	00180-7337	H	
227	00 18 49.3	-74 52 38	5 -	- -	1.5 -	- -	-	0.19:	-	0.6:	-	00188-7452	H:	
228	00 19 56.4	-74 26 10	- -	4 -	12 -	3 -	p:	-	0.44	4.9	6.2	00199-7426	C	
229	00 21 53.8	-73 54 00	- -	2 -	- -	- -	-	-	0.22	-	-	00218-7353	H	N 1, Sk 1
230	00 22 07	-74 34	- -	- -	- -	0.5 -	-	-	-	-	1.0		C	
231	00 22 31	-74 21	- -	- -	- -	0.5 -	-	-	-	-	1.0		C	
232	00 25 03	-74 35	- -	- -	- -	0.7 -	-	-	-	-	1.5		C	
233	00 26 03.0	-73 15 18	6 -	20 -	16 -	1.5 -	p	0.22	2.20	6.6	3.1	00260-7315	H	
234	00 26 28.0	-74 37 47	- -	- -	1.5 -	0.5 -	p:	-	-	0.6	1.0	00264-7437	C	
235	00 26 37	-73 56	- -	2 -	- -	- -	p	-	0.22	-	-		H	
236	00 27 20	-74 12	- -	- -	1.5 -	1 -	-	-	-	0.6	2.1		C	
237	00 27 40	-74 20	- -	- -	1 -	0.5 -	-	-	-	0.4	1.0		C	
238	00 28 05	-74 29	5 -	- -	- -	- -	p	0.19	-	-	-		S	
239	00 29 37.0	-74 04 17	- -	2 -	4 -	1.5 -	p	-	0.22	1.6	3.1	00296-7404	C	DEM 1, N 3
240	01 26 16	-73 31	5 -	- -	2 -	1 -	p:	0.19	-	0.8	2.1		C	DEM 167
241	01 27 47	-73 30	- -	- -	1 -	1 -	-	-	-	0.4	2.1		C	DEM 167
242	01 28 23.1	-73 49 17	- -	6 -	22 -	12 -	2xp	-	1.05	11.1	27.2	01283-7349 X0128-738	C	DEM 166
243	01 28 43	-74 10	- -	- -	- -	0.5 -	-	-	-	-	1.0		C	
244	01 29 07.7	-73 25 38	6 -	2 -	- -	- -	p:	0.22	0.22	-	-	01291-7325	S:	SAO 255786
245	01 29 08	-73 28	- -	- -	- -	0.5 -	-	-	-	-	1.0		C	DEM 167
246	01 31 19.7	-73 42 30	- -	- -	1 -	1.5 -	p:	-	-	0.4	3.1	01313-7342	C	DEM 167
247	01 33 06.0	-73 21 00	5 -	- -	- -	- -	p:	0.19	-	-	C	01331-7321	S	
248	01 41 26	-73 33	- -	- -	- -	0.5 -	-	-	-	-	1.0		C	
249	01 41 38.5	-73 43 12	- -	- -	- -	0.5 -	p:	-	-	-	1.0	01416-7343	C	

TABLE A.3. — *SAO (1966) stars in the additional SMC fields.*

(1) SAO number	(2) m V mag	(3) Sp type	(4) F[a] 12μm Jy	(5) F[a] 25μm Jy	(6) F 25μm /F 12μm	(7) m - m V 12 mag	(8) Infrared Id	(9) Detection[b] quality	(10) Remarks[c]
255653	8.0	G5	0.13:	0.16:	1.2 ±1.0	2.2	220	0	On edge of Co-added map.
255665	8.8	G5	0.08	0.08:	1.0 ±1.0	2.4		0	
255675	9.2	A	-	-	-	-		-	
255786	8.3	K0	0.16	0.16	1.0 ±1.0	2.7	244	+	
255793	9.0	G5	-	-	-	-		-	
255805	9.3	--							Not covered by Co-added map.
255807	9.2	--							Not covered by Co-added map.

Notes to Table A.3:
a) The 12 and 25 μm flux densities in this table are colour-corrected (see Table 5).
b) Detection qualities at 12 μm are good (+), medium (0) or poor (-).
c) See Section A.5.1.1 in Appendix A.

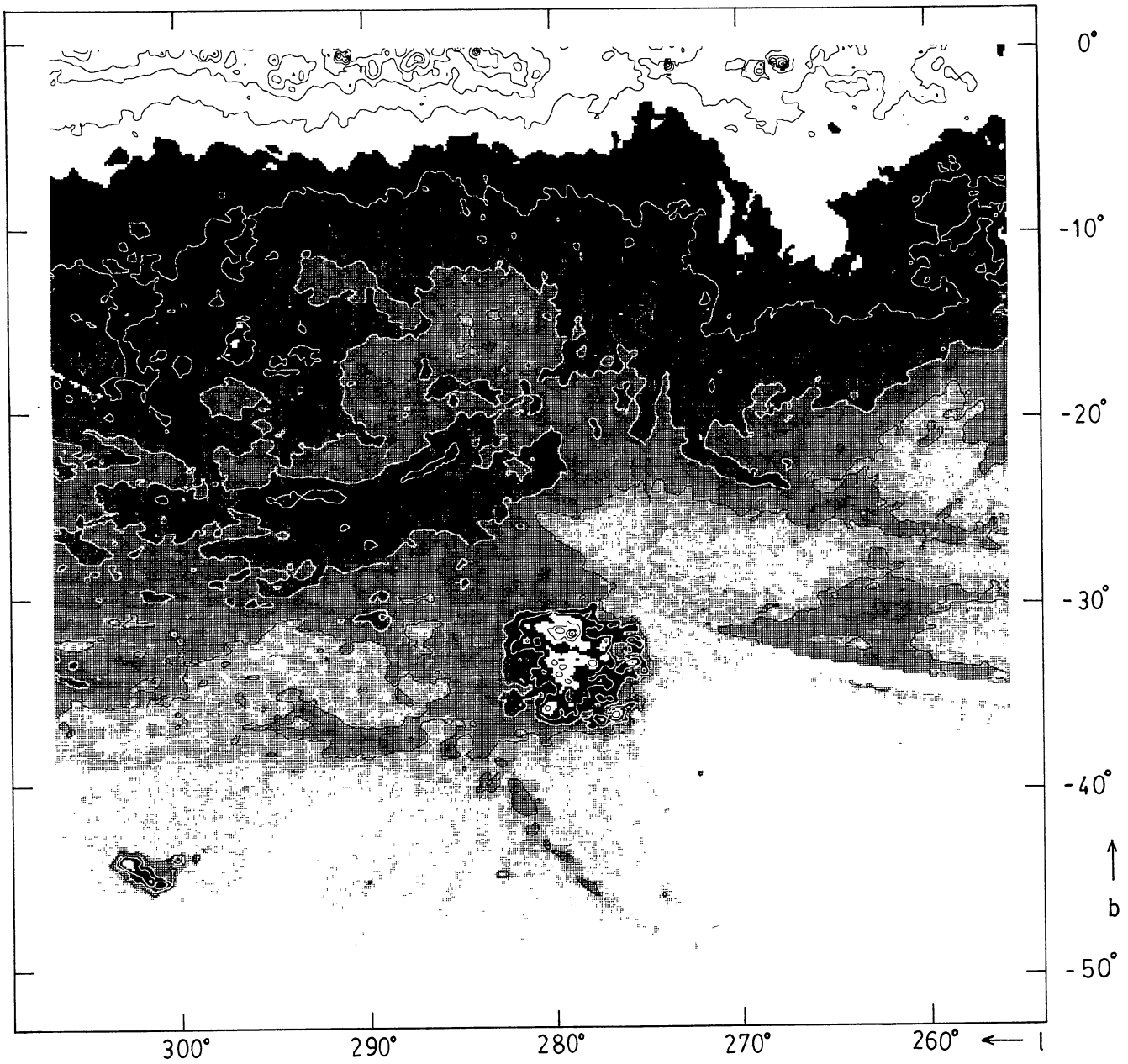

FIGURE 1. — IRAS Spline-I infrared map at 100 μm made at the Groningen Laboratory for Space research (van Albada *et al.*, 1985 ; Braun, Walker and Deul, priv. comm.) showing an area of 50° × 50° around the Magellanic Clouds with a resolution of about 10′. Galactic 1950 coordinates are indicated. The infrared foreground can clearly be seen. Two extended infrared features (tidal arms) are in fact associated with HI at local Galactic velocities. Intensities between 4 and 35 Watt m^{-2} sr^{-1} are indicated by grey scales, with darker grey scales for higher intensities. Contours are at 11, 14, 21, 70, 175, 350, 700, 1750, 3500, 5250 × 10^{-8} Watt m^{-2} sr^{-1}.

FIGURE 2. — Overall infrared maps of the Small Magellanic Cloud. Map set 2 (NS) of table II is presented in equatorial coordinates for 1950. The maps are given in in-band intensities. All maps have sizes of 4°.3 × 4°.3. The coverage of the DPM-field is indicated by solid lines. Although not shown, the coverage differs somewhat in the four wavelength bands due to the location of detectors in IRAS's focal plane. For the 12 μm band grey scales range from 9 to 33, with darker grey scales for higher intensities. Contours are at 5, 10, 15, 20, 50 × 10^{-8} Watt m^{-2} sr^{-1}. For the 25 μm band grey scales range from 9 to 33, with darker grey scales for higher intensities. Contours are at 2, 4, 6, 8, 10, 30, 50, 100 × 10^{-8} Watt m^{-2} sr^{-1}. For the 60 μm band grey scales range from 9 to 58, with darker grey scales for higher intensities. Contours are at 1, 2, 4, 6, 8, 10, 15, 20, 40, 80, 140, 200 × 10^{-8} Watt m^{-2} sr^{-1}. For the 100 μm band grey scales range from 9 to 58, with darker grey scales for higher intensities. Contours are at 0.5, 1, 2, 4, 6, 8, 10, 15, 20, 40, 80 × 10^{-8} Watt m^{-2} sr^{-1}. ⟶

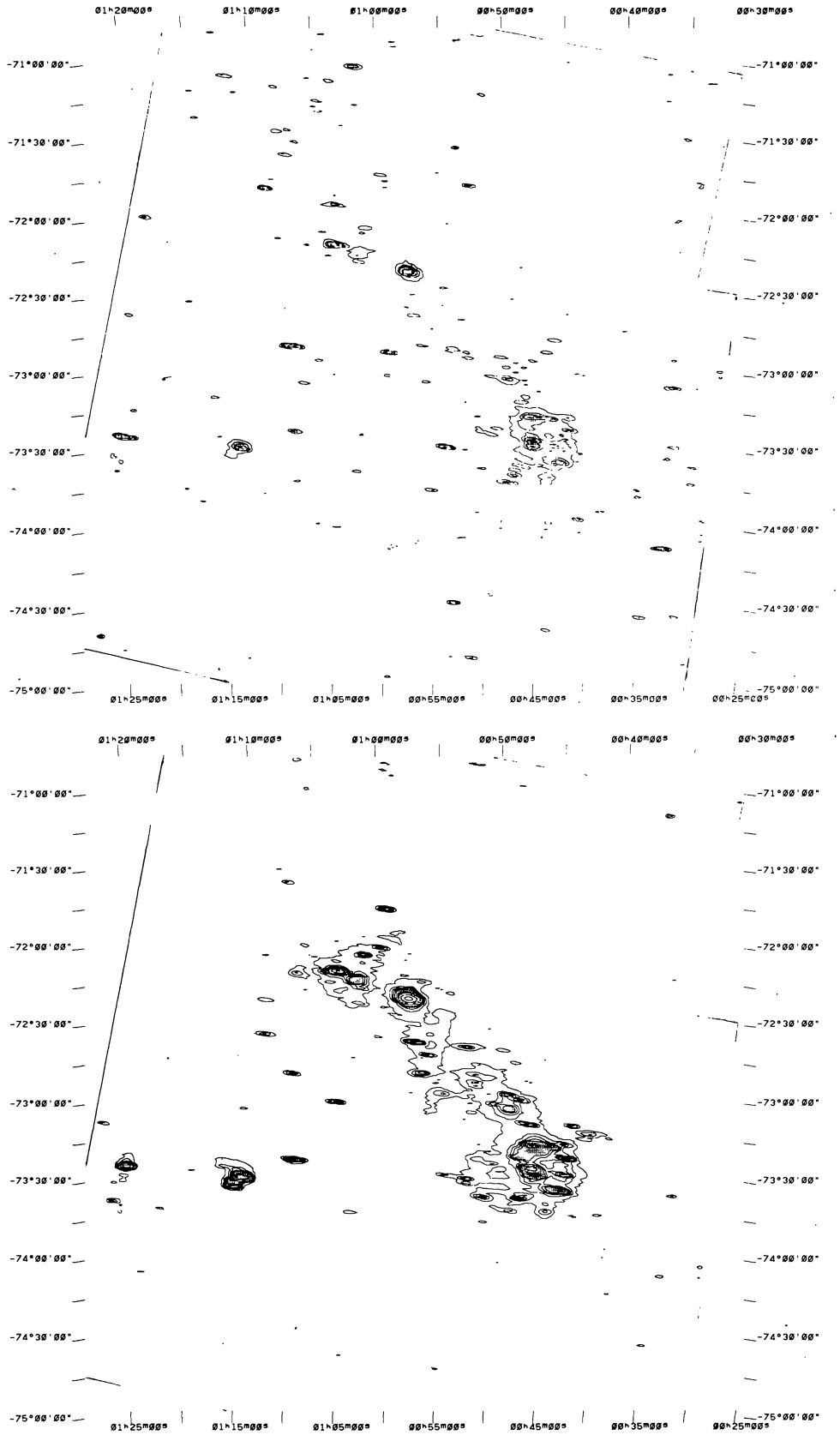

FIGURE 2.1. — SMC 12 μm DPM-map (set 2 ; NS).

FIGURE 2.2. — SMC 25 μm DPM-map (set 2 ; NS).

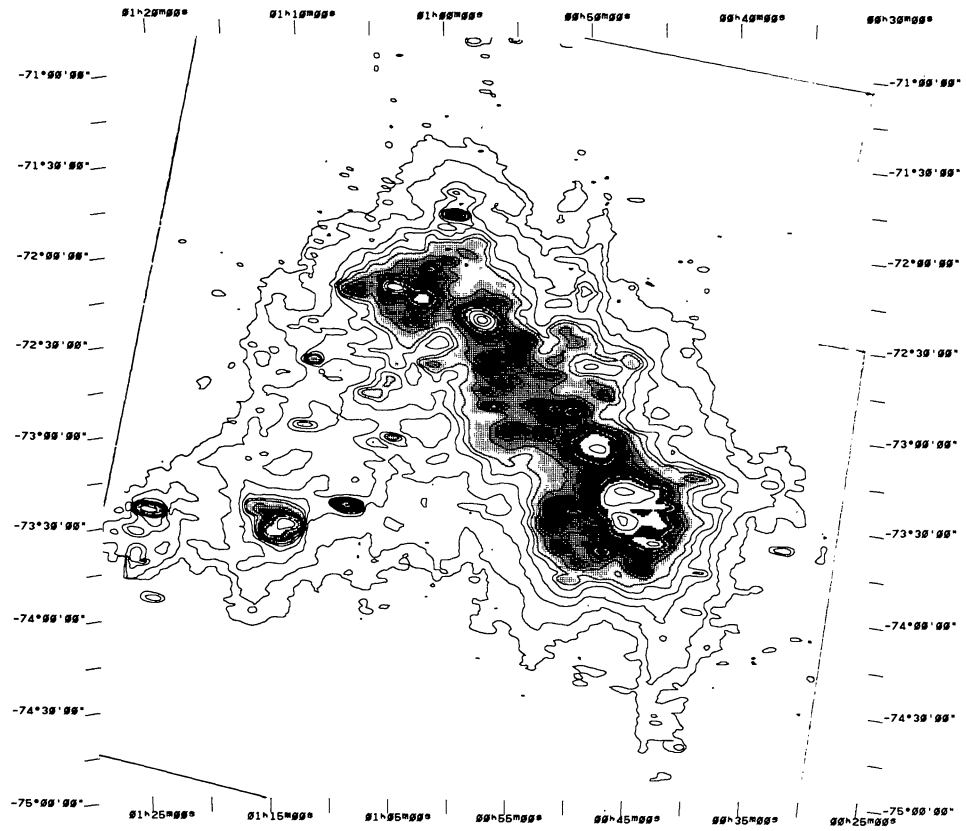

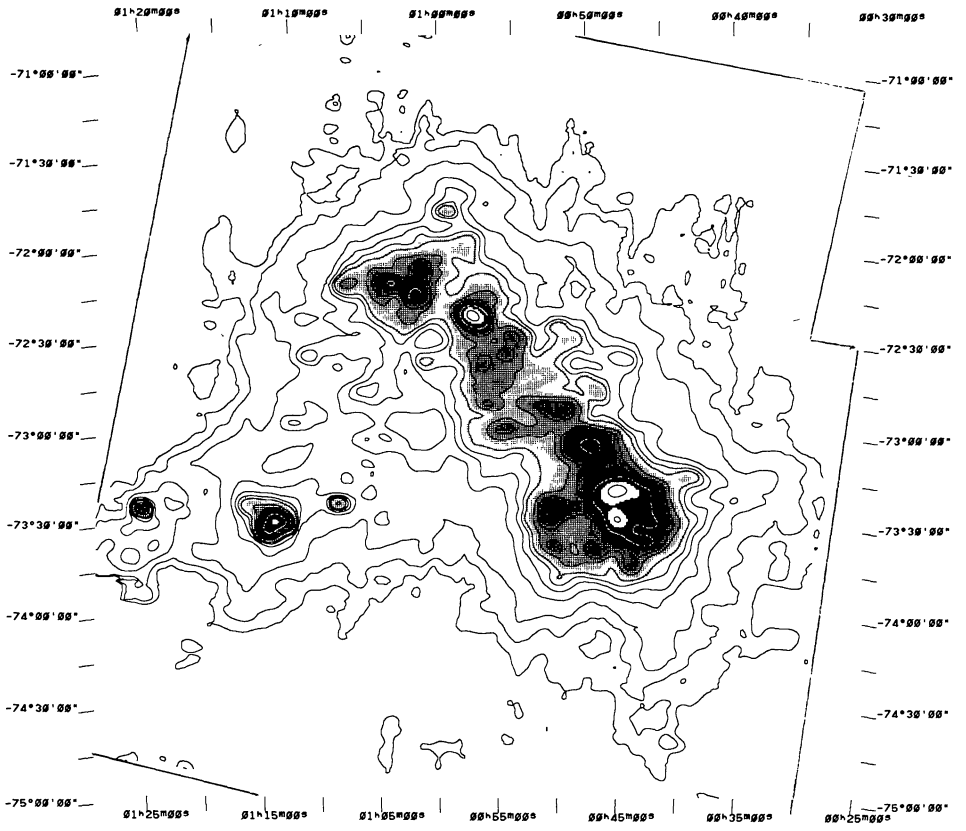

FIGURE 2.3. — SMC 60 μm DPM-map (set 2 ; NS).

FIGURE 2.4. — SMC 100 μm DPM-map (set 2 ; NS).

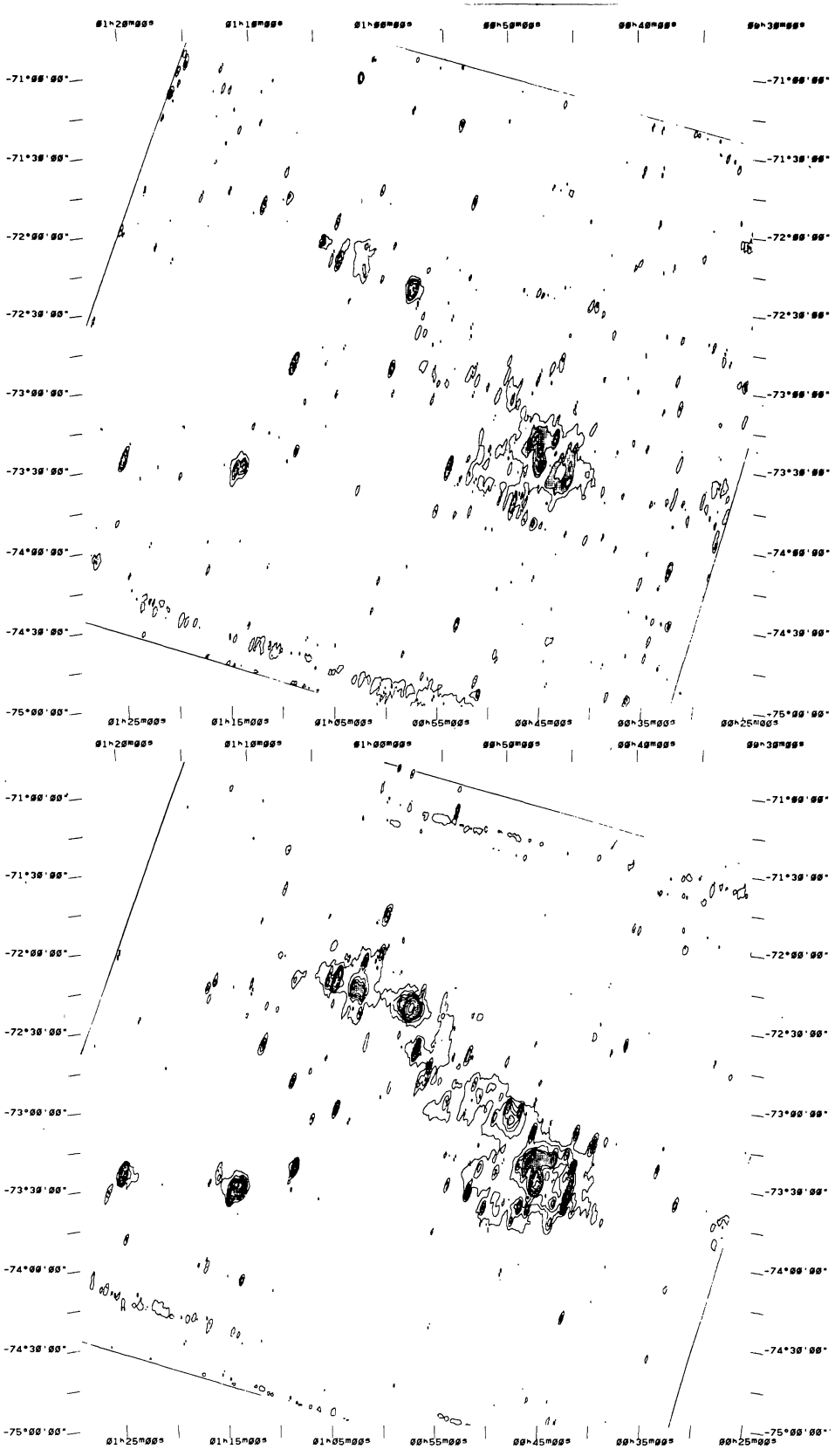

FIGURE 3.1. — SMC 12 μm DPM-map (set 3 ; EW).

FIGURE 3.2. — SMC 25 μm DPM-map (set 3 ; EW).

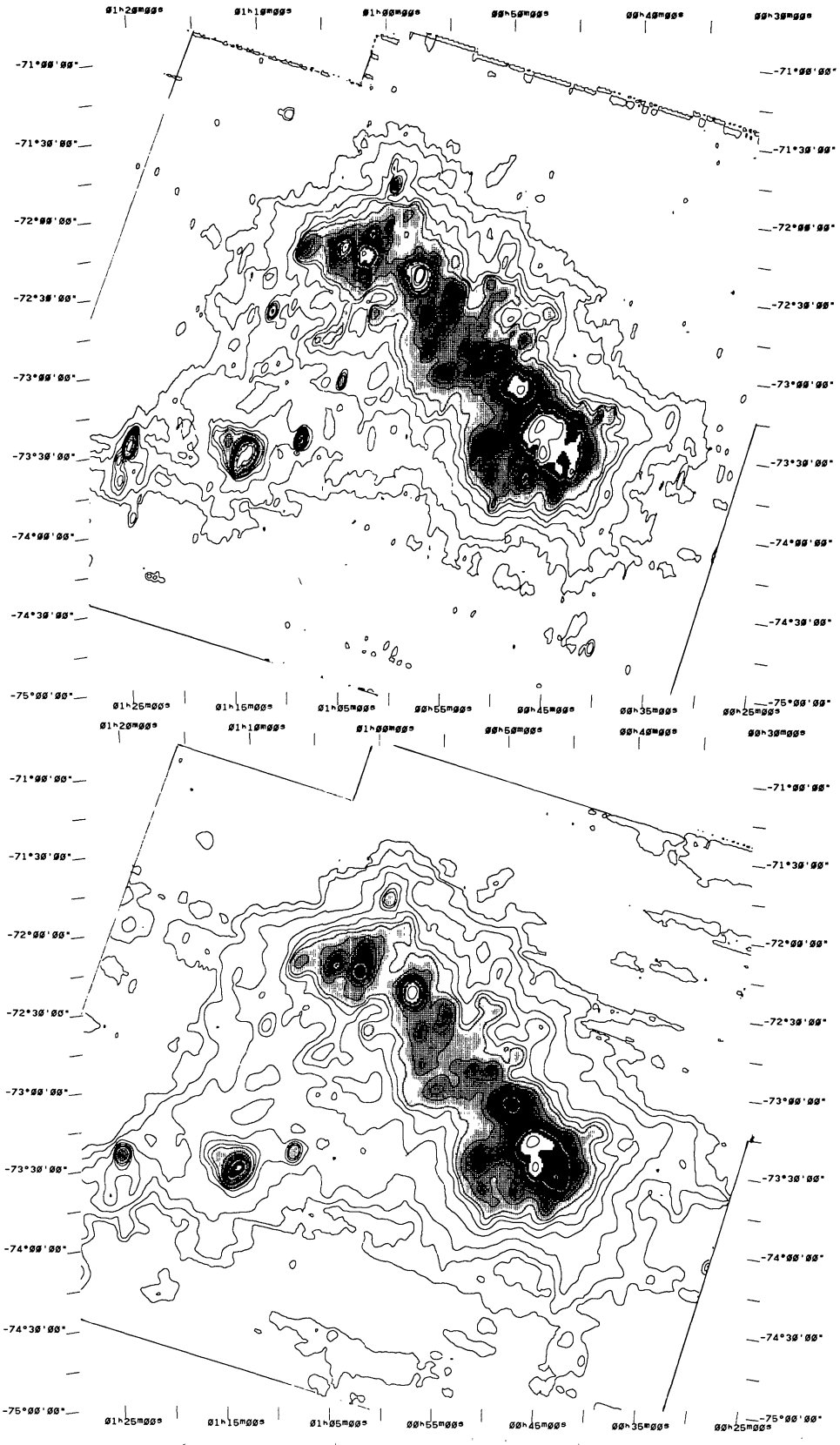

FIGURE 3.3. — SMC 60 μm DPM-map (set 3 ; EW).

FIGURE 3.4. — SMC 100 μm DPM-map (set 3 ; EW).

FIGURE 3. — Overall infrared maps of the Small Magellanic Cloud. Map set 3 (EW) of table II is presented in an identical way as set 2 (NS) in figure 2. The coverage of the DPM-field is indicated by solid lines.